

UNIVERSITY OF CALIFORNIA

Los Angeles

Mass Transfer at Contaminated Bubble Interfaces

A dissertation submitted in partial satisfaction of the
requirements for the degree Doctor of Philosophy
in Civil Engineering

by

Diego Rosso

2005

The dissertation of Diego Rosso is approved.



Jenny A. Jay



Keith D. Stolzenbach



Yoram Cohen



Michael K. Stenstrom, Committee Chair

University of California, Los Angeles

2005

TABLE OF CONTENTS

LIST OF FIGURES	iv
LIST OF TABLES.....	v
ACKNOWLEDGEMENTS.....	vi
VITA.....	vii
ABSTRACT.....	viii
1. INTRODUCTION	1
2. LITERATURE REVIEW	4
2.1. Gas transfer.....	4
2.1.1. The Clean Water Test	6
2.1.2. Corrections to Non-Ideal Conditions.....	9
2.1.3. Oxygen Absorption into Agitated Liquids.....	11
2.2. Bubble mechanics.....	12
2.2.1. Dynamics of Bubble Formation.....	12
2.2.2. Surface Tension and its Measurements.....	16
2.2.3. Internal Circulation Phenomena	19
2.2.4. Bubble - Bubble Interactions	21
2.3. Surface Active Agents	22
2.3.1. Classification and Properties.....	22
2.3.2. Liquid Side: Adsorption at Gas - Liquid Interfaces.....	24
2.3.3. Gas Side: Effects on Oxygen Transfer.....	32
2.4. Experimental Observations.....	35
2.4.1. Effects on Dynamic Surface Tension	35
2.4.2. Effects on Terminal Velocity.....	38
2.4.3. Effects on the Mass Transfer Coefficient	39
2.5. Summary.....	43
3. EXPERIMENTAL DATASETS	46
3.1. Data from Masutani (1988)	46
3.2. Data from Huo (1998)	47
3.3. Equilibrium Surface Tension Measurements.....	47
3.4. Dynamic Surface Tension Measurements	48
3.5. Mass Transfer Coefficient Measurement.....	51
3.6. Remarks on Raw Data	53
4. RESULTS AND DISCUSSION	57
4.1. Preliminary Results.....	57
4.2. Discussion.....	65
4.3. Dimensionless Presentation of Results.....	72
5. SUMMARY AND CONCLUSIONS	86
6. FURTHER RESEARCH	88
7. REFERENCES	89
8. APPENDIX.....	100

LIST OF FIGURES

Figure 2.1. Batch system model for the Clean Water Test	6
Figure 2.2. Sample Clean Water Test: dissolved oxygen vs. time	8
Figure 2.3. Map of single bubble shape regimes in a Newtonian fluid	15
Figure 2.4. The du Noüy ring testing apparatus.....	16
Figure 2.5. Internal bubble circulation and surface tension gradients	19
Figure 2.6. Schematic drawing and molecular model for sodium lauryl sulfate	23
Figure 2.7. The two ways of SAA molecular stabilization.....	24
Figure 2.8. Interfacial monolayer and foaming effect	25
Figure 2.9. Dimensionless characteristic curve for sodium dodecyl sulfate.....	27
Figure 2.10. Integration domain for a forming bubble	28
Figure 2.11. Volumetric mass transfer coefficient ($k_L a$) and velocity of adsorption (k_L) in solutions with various concentrations of sodium lauryl sulfate	33
Figure 2.12. Surface tension as a function of SAA additions.....	36
Figure 2.13. Dynamic surface tension of Tergitol and sodium dodecyl sulfate	37
Figure 2.14. Terminal velocities for air bubbles in water and contaminated liquids.....	38
Figure 2.15. Drag coefficient for air bubbles as a function of the Reynolds number.....	39
Figure 2.16. Mass transfer effects: enhancement by salts and aliphatic alcohols.....	40
Figure 2.17. Mass transfer effects: depression by antifoam agents and surfactants	41
Figure 2.18. Mass transfer effects: effects on the mass transfer coefficient.....	43
Figure 3.1. Dynamic surface tension measuring apparatus	49
Figure 3.2. Typical bubble formation pattern	51
Figure 3.3. Aeration apparatus.....	52
Figure 3.4. Sample DST measurement on Tergitol solutions.....	54
Figure 3.5. Mass transfer coefficient measurements	56
Figure 4.1. Dynamic surface tension and interfacial excess accumulation for sodium dodecyl sulfate	58
Figure 4.2. Surface accumulation calculated with the Langmuir and Ward-Tordai adsorption models	60
Figure 4.3. Concurrent interfacial phenomena for a single bubble.....	62
Figure 4.4. Concurrent DST and mass transfer measurements.....	63
Figure 4.5. Flow regime effects on mass transfer time-series	68
Figure 4.6. Schematics of surfactant interfacial accumulation and its reduction of gas turbulence	69
Figure 4.7. Comparison of fine- and coarse-bubbles generated by two different aerators operating at same airflow rate	71
Figure 4.8. Results of the statistical analysis: plot of (Sh) versus estimated (Sh)	79
Figure 4.9. Dimensionless representation of mass transfer phenomena with time.....	81
Figure 4.10. Dimensionless characterization of mass-transfer phenomena at a fine-bubble interface.....	83
Figure 4.11. Comparison of (Sh) from experimental data, a data fit calculated with a Frössling-like equation, and a data fit calculated with eq.4.6.....	85
Figure 4.12. Limits of applicability of eq.4.6: (Sh) vs. (Pe)	86

LIST OF TABLES

Table 2.1. Summary of available literature sources.....	44
Table 4.1. Dimensional matrix.....	74
Table 4.2. Dimensionless numbers, notation and physical significance.....	75
Table 4.3. Results of the statistical analysis: estimated vs. calculated (Sh)	78

ACKNOWLEDGEMENTS

I thank G. Masutani and D.L. Huo for their patience and skill in conducting the experiments that produced the data analyzed in this research. I also thank the members of my doctoral committee, Profs. Jay, Stolzenbach, and Cohen, all the professors I had in this university, the staff, and my co-workers for all the things I learnt from them. I also thank Dr. Iranpour, co-author of one of my publications.

I acknowledge the California Department of Transportation, Southern California Edison, and the California Energy Commission for financial support.

The Appendix contains reprints of my publications. I kindly thank the publishers for granting reprint permission. Copyrights are owned by Water Environment Federation for:

Economic Implications of Fine Pore Diffuser Aging, *Water Environment Research*, in press.

Fifteen years of OTE measurements on fine pore aerators: key role of sludge age and normalized air flux, *Water Environment Research*, 77(3) 266-273.

and Elsevier Publishing for:

Comparative Economic Analysis of the Impacts of Mean Cell Retention Time and Denitrification on Aeration Systems, *Water Research* 39, 3773-3780.

Surfactant Effects on Alpha Factors in Full-Scale Wastewater Aeration Systems, *Water Research*, in press.

Finally, I thank my advisor, towards whom I have an incommensurable debt of gratitude, for teaching me that “Young minds must be educated with wisdom, not by force”

(Publius Sirius).

VITA

- 1976 Born, Verona, Italy
- 2002 *Laurea*, Chemical Engineering
University of Padua, Italy
- 2003 M.S., Civil Engineering
University of California, Los Angeles
- 2003-2004 Teaching Assistant
Civil and Environmental Engineering Department
University of California, Los Angeles
- 2002-2005 Graduate Student Researcher
Civil and Environmental Engineering Department
University of California, Los Angeles

PUBLICATIONS AND PRESENTATIONS

- Rosso, D. and Stenstrom, M.K. (2005) Comparative Economic Analysis of the Impacts of Mean Cell Retention Time and Denitrification on Aeration Systems, *Water Research* 39, 3773-3780.
- Rosso, D. and Stenstrom, M.K. (2005) Economic Analysis of Aeration System Retrofits in Biological Nutrient Removal Activated Sludge Processes, *Proceedings of the IAW Nutrient Management in Wastewater Treatment Conference*, Krakow (Poland).
- Rosso, D. and Stenstrom, M.K. (2005) Economic Implications of Fine Pore Diffuser Aging, *Water Environment Research*, in press.
- Rosso, D. and Stenstrom, M.K. (2005) Economic Implications of Fine Pore Diffuser Ageing, *Proceedings of the 78th WEFTEC Conference*, Washington, DC (USA).
- Rosso, D., Iranpour, R., and Stenstrom, M.K. (2001) Oxygen Transfer Efficiency: Fifteen Years of Off-Gas Testings, *Proceedings of the 73rd WEFTEC Conference*, Atlanta, GA (USA).
- Rosso, D., Iranpour, R., and Stenstrom, M.K. (2005) Fifteen years of OTE measurements on fine pore aerators: key role of sludge age and normalized air flux, *Water Environment Research*, 77(3) 266-273.

ABSTRACT OF THE DISSERTATION

Mass Transfer at Contaminated Bubble Interfaces

by

Diego Rosso

Doctor of Philosophy in Civil Engineering

University of California, Los Angeles, 2005

Professor Michael K. Stenstrom, Chair

Aeration is an essential process in the majority of wastewater treatment processes, and accounts for the largest fraction of operating costs. Aeration systems can achieve gas transfer by shearing the surface (surface aerators) or releasing bubbles at the bottom of the tank (coarse- or fine-bubble aerators). The effectiveness of gas transfer processes is reduced by the presence of dissolved contaminants, i.e. surface active agents, in the liquid medium.

Surface active agents accumulate at gas-liquid interfaces, and reduce mass transfer rates. This reduction in general is larger for smaller bubbles. Surface active agents are present as measurable trace contaminants at all environmental and at most industrial gas-liquid interfaces. The quantification of gas transfer depression caused by surface active agents is necessary to calculate increased energy costs when designing and specifying aeration systems.

Datasets from previous experiences in our laboratory were assembled and analyzed in this study. These included concurrent measurements of dynamic surface tension and mass transfer coefficients. Data were recorded in both time-dependent and time-integrated experiences. In this work, the parameters describing the evolution of bubble interfacial contamination over time were also enclosed. This was done by calculating surfactant interfacial accumulation, surfactant surface diffusivity, and corrected interfacial gas diffusivity for each bubble surface age using a time-dependent adsorption model.

A dimensional analysis was performed on the system, resulting in correlations that present the results in dimensionless fashion. The resulting correlations were statistically significant. Results are consistent with expectations and correct previous Frössling-like dimensionless correlations for systems without contamination. The results formally describe observed transport phenomena, and offer a tool for mass transfer prediction from flow regime and dynamic surface tension properties.

1. INTRODUCTION

Gas-liquid reactors have extensive application in industrial and environmental fields.

Several technologies are available for generating gas-liquid interfaces. Aeration devices transfer gas to a liquid media by either creating a gas-liquid interface or using a semi-permeable membrane that allows the dissolution of gas into the liquid without the formation of an interface. Environmental applications usually rely on the former method, where the gas-liquid interface is created by either shearing the liquid surface into droplets with a mixer or turbine, or by releasing air through spargers (producing coarse bubbles), porous sintered ceramic materials or punched polymeric membranes (producing midrange or fine bubbles, according to ceramic granulometry and gas flowrate).

Falling droplets and rising coarse bubbles have large interfacial gas-liquid velocity gradients and can be grouped as high flow regime interfaces, whereas fine bubbles have low interfacial velocity gradients and can be grouped as low flow regime interfaces. In environmental applications, it is customary to consider coarse the bubbles with a diameter larger than 50 μm , and fine the bubbles with a diameter smaller than 5 μm .

Porous sintered materials and polymeric punched membranes are usually referred to as fine pore diffusers. Novel technologies (referred to as bubbleless) adopt “true” semi-permeable membranes, such as membranes used for microfiltration, which allow the transport of water and air across the membrane, without permitting the passage of solute or suspended matter (Côté et al, 1989; Semmens, 1990).

Aeration is an essential process in the majority of wastewater treatment processes, and accounts for the largest fraction of plant energy costs, ranging from 45 to 75 % of the operating cost (Reardon, 1995; Rosso and Stenstrom, 2005a). Fine pore diffusers have become the most common aeration technology in wastewater treatment in the United States and Europe, and have higher efficiencies per unit energy consumed (Standard aeration efficiency or SAE, $\text{kgO}_2\cdot\text{kWh}^{-1}$). They are usually installed in full floor configurations, which enhance their operating efficiency. Fine-pore diffusers have two important disadvantages: the need for periodic cleaning, and the large negative impact on transfer efficiency from wastewater contaminants. The implications of diffuser ageing and the benefits of cleaning have been discussed (Rosso and Stenstrom, 2005b).

Environmental processes are characterized by the presence of a variety of contaminants, both hydrophobic and hydrophilic. The most frequently occurring contaminants in environmental mass-transfer applications are surface active agents. The chemical nature of surface active agents causes their accumulation at gas-liquid interfaces, which results in reduced gas transfer rates. The impact of contamination on aeration performance is usually quantified by the α factor (ratio of process water to clean water mass transfer coefficients), defined and discussed in chapter 2.

Mass transfer depression caused by contaminants has long been observed (Kessener and Ribbius, 1934; Mancy and Okun, 1960). Lower flow regime gas-liquid interfaces (such as the ones produced by fine-pore diffusers) generally have lower α factors than higher flow regime interfaces (such as the ones produced by coarse bubble diffusers or surface

aerators) for similar conditions (Stenstrom and Gilbert, 1981). This is because surfactants are more effective at low interfacial velocity gradients.

The effects of wastewater contamination on mass transfer can be related to the decrease in dynamic surface tension (Eckenfelder, 1959; McKeown and Okun, 1961; Masutani and Stenstrom, 1991). The interfacial accumulation of surfactants causes an increase in interfacial rigidity (hence in the drag coefficient), the reduction of internal gas circulation, and the reduction of interfacial renewal rates. There exists a variety of gas transfer models for pure fluid systems (Lewis and Whitman, 1924; Higbie, 1935; Danckwerts, 1951). Empirical correlations for pure systems are also available (Frössling, 1938). Gas transfer models and empirical correlations for pure liquids do not predict the reduction in transfer rates caused by surfactants.

Objective of this work is to quantify the effects of surfactant accumulation at bubble interfaces. Datasets from previous experiences in our laboratory were assembled and analyzed. These included both early and mature interfacial formation stages. The datasets contain concurrent dynamic surface tension and mass transfer coefficient measurements, collected with single- and multi-bubble aeration apparatuses. In this fashion, both time-dependent and time-averaged data were represented. A dimensional analysis was performed and previous empirical observations were confirmed and corrected. The outcomes of the dimensional analysis are empirical correlations, which quantify the reduction of mass transfer rates due to interfacial surfactant contamination.

2. LITERATURE REVIEW

Following is the review of the main areas of interest in this study. The order of presentation follows a logical path, from the general to the detailed view of the phenomena. First, it is presented the most diffused and approximated modeling of oxygen transfer, the one adopted for clean water tests. Secondly, going into more detail, single bubble phenomena are described. Thirdly, the phenomena occurring at the bubble interface are reported. The last section reviews the available experimental data that will be used to test the model proposed in this work.

2.1. Gas transfer

The efficient operation of biological reactors strictly relies upon an effective aeration system. Oxygen provides the aerobic microbes with an electron acceptor for sustain of life as well as for the engineered process (Bailey and Ollis, 1986). In wastewater engineering this knowledge has been applied in order to optimize pollutant removal and minimize energy expenditure (US EPA, 1985, 1989). A compendium of oxygen absorption applied to wastewater treatment is here presented.

The theory of gas-liquid absorption has been extensively applied to model oxygen transfer, with further refinements (Bird et al., 1960; Treybal, 1968; Sherwood et al., 1975; Danckwerts, 1970). There are several experimental correlations that describe the mass

transfer from a bubble to the surrounding liquid (Carver, 1969; Chang and Franses, 1994)., due to the solid bubble approximation (Boussinesq, 1913).

Mass transfer models for pure fluids are well-known and are based on the solid-sphere (Boussinesq, 1913) or the fluid sphere (Prandtl, 1934) approximation. Motarjemi and Jameson (1978) observed with experiments that mass transfer coefficients are higher than the predictions with the solid sphere model, indicating moving gas-liquid interfaces. The most common gas-transfer models are the stagnant two-film model (Lewis and Whitman, 1924), the penetration theory (Higbie, 1935) and the surface renewal model (Danckwerts, 1951). Both the penetration theory and the surface renewal models account for the liquid agitation, thus embodying the flow regime parameters into the mass transfer calculation. Depending on the flow regime, these models can predict mass transfer of pure gas-liquid systems with accuracy. Mass transfer models for spherical interfaces refer back to the earliest studies of mass transfer between fluids and a solid sphere (Frössling, 1938; Friedlander, 1961; Griffith, 1960; Levich, 1959, 1962; Johnson et al., 1967). There also exist analytical solutions to the problem of mass transfer from falling pure spheres in laminar flow regime derived from the boundary layer theory (Friedlander, 1957).

The Lewis and Whitman model is extensively applied with success in evaluating aeration devices for environmental purposes (ASCE, 1984, 1991; ATV-DVWK 1996; prEN 12255-15, 1999). When analyzing gas transfer, the efficiency of the aeration devices plays a key role. In the case of surface contamination, process mass transfer coefficients decrease to values well-below the ones measured in clean water (Mancy and Okun, 1960).

Experimental evidence shows that a stagnant film approach may not be suitable for moving gas-liquid interfaces, when comparing bubbles into clean and contaminated liquid solutions. (Eckenfelder, 1959; Eckenfelder and Barnhart, 1961).

2.1.1. The Clean Water Test

The need for standardization and comparability in oxygen transfer estimates led to the development of testing protocols (ASCE, 1984, 1991, 1997; ATV-DVWK 1996; prEN 12255-15, 1999). The ASCE protocol, as an example, describes the procedure to evaluate the gas-liquid mass transfer coefficient $k_L a$, i.e. the parameter that quantifies the velocity of absorption. This mass transfer model assumes the interfacial films to be stagnant with only diffusional transport across the interface (Lewis and Whitman, 1924). If we consider the batch system in Figure 2.1, the material balance on the dissolved oxygen is:

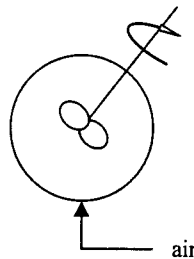


Figure 2.1. Batch system model for the Clean Water Test

$$\frac{dc}{dt} = k_L a \cdot (c_\infty^* - c) \quad (2.1)$$

where k_La = overall mass transfer coefficient (T^{-1})

c = dissolved oxygen concentration at time t ($M \cdot L^{-3}$)

c_{∞}^* = equilibrium oxygen concentration at saturation = 9.08 mg/l @ $T = 20$ °C

In the Clean Water Test, oxygen is first sequestered with sodium sulfite, using cobalt chloride as a catalyzer:



Following the oxygen segregation, which occurs almost instantaneously, the aeration device provides air to the batch system and, when the excess sodium sulfite is completely converted into sulfate as in Eq. 2.2, the system experiences re-aeration (hence the name “re-aeration test” that can be used *in lieu* of “Clean Water Test”) which is quantified by integrating (2.1) with the condition $c = c_i$ @ $t = 0$,

$$c = c_{\infty}^* - (c_{\infty}^* - c_i) \cdot e^{-k_La \cdot t} \quad (2.3)$$

Estimates of k_La and c_i can be obtained by fitting experimental data with an exponential, a differential or a loglinear fit (Stenstrom and Gilbert, 1981). The error present in estimated values can be minimized by using a composite predictive method (Philichi and Stenstrom, 1989). First, the equilibrium concentration is estimated with an exponential fitting model (Eq. 2.3), and the initial values of dissolved oxygen concentration are

truncated for this purpose. Secondly, the estimated equilibrium concentration obtained from Eq. 2.3 is used in the log deficit form of the solution to Eq. 2.1:

$$\ln\left(\frac{c_{\infty}^* - c}{c_{\infty}^* - c_i}\right) = -k_L a \cdot t \quad (2.4)$$

which is more accurate at estimating $k_L a$ (slope of the loglinear trend) than Eq. 2.3. This calculation can be performed using the ASCE DO Parameter Estimation Program (DO_PAR) software available at <http://fields.seas.ucla.edu/research/dopar/> for download.

Figure 2.2 shows the evolution over time of a sample Clean Water Test performed in our laboratory. Dissolved oxygen concentrations were sampled at a frequency of 0.2 s^{-1} .

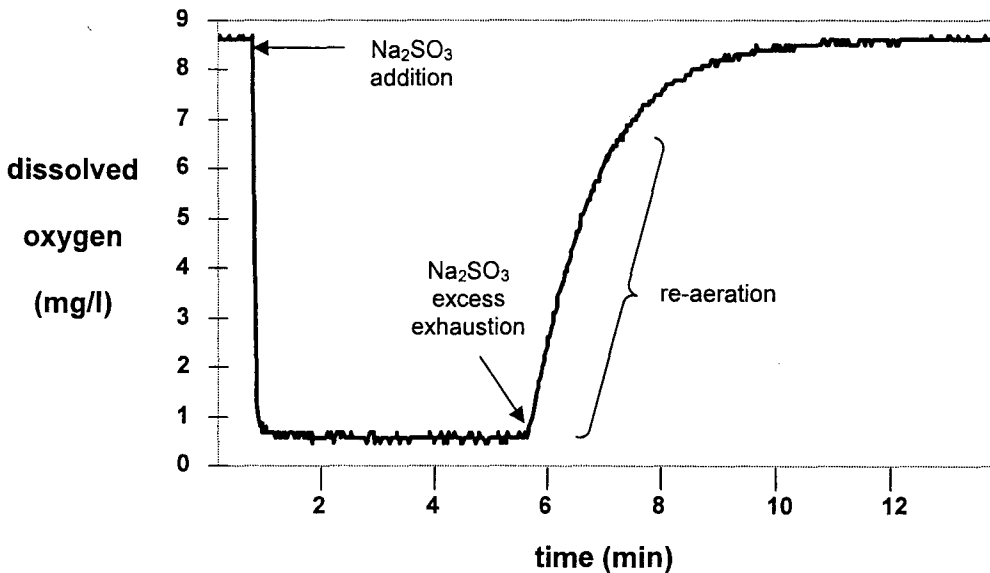


Figure 2.2. Sample Clean Water Test: dissolved oxygen vs. time.

The first rapid decline of dissolved oxygen concentration corresponds to the addition of sodium sulfite and cobalt chloride. After a steady-state plateau, where the excess sulfite is converted to sulfate, the concentration increases (re-aeration process).

2.1.2. Corrections to Non-Ideal Conditions

In order to compare different results it is necessary to account for the difference in process conditions. The main variables that affect oxygen transfer estimates are listed in the ASCE standard guidelines (ASCE, 1984, 1991, 1997). Three parameters are commonly used, α , β , and θ , which account respectively for mass transfer coefficient, salinity, and temperature corrections (Stenstrom and Gilbert, 1981):

$$\alpha = \frac{(k_L a)_{pw}}{(k_L a)_{cw}} \quad (2.5)$$

$$\beta = \frac{c_{\infty, pw}^*}{c_{\infty, cw}^*} \quad (2.6)$$

$$\theta^{(T-20^\circ C)} = \frac{k_L a(T)}{k_L a(20^\circ C)} \quad (2.7)$$

where $k_L a$ is the volumetric mass transfer coefficient (time^{-1}), c_{∞}^* is the oxygen concentration at saturation, and the subscripts pw and cw stand for process water and clean (tap) water, respectively. Errors in the evaluation of α can be crucial for the design and verification of a wastewater treatment process, while the other two parameters are easier to quantify (Stenstrom and Gilbert, 1981). A key reason behind the difficulty in α

assessments lies in its definition. The two film theory adopted for the derivation of α assumes stagnant gas and liquid films (Lewis and Whitman, 1924), and the mass transfer coefficient will only be a function of the molecular diffusivity of the gas into the liquid:

$$k_L a \sim \mathcal{D} \quad (2.8)$$

where \mathcal{D} is the gas diffusivity. In the two-film theory, the transport from the gas bulk to the liquid bulk is postulated to occur by molecular diffusion only, with no accumulation or advection assumed at the interfacial films. For sparingly soluble gases, by definition, the liquid film resistance controls the transport, and the interfacial gas concentration can be estimated by Henry's law.

The stagnant film assumption is a restriction that can be offset by several operating conditions. Different aeration technologies (i.e. surface mixers, fine bubble diffusers) are characterized by different ranges of α (Eckenfelder and Ford, 1968). This is due to the fact that at higher energy expenses, a higher shear rate can overcome diffusional bottlenecks offering highly turbulent interfacial films (Hwang and Stenstrom, 1979). Amongst fine bubble diffusers, although, there is no evidence that correlates different α values to different diffuser designs and technologies (Rosso et al., 2001; 2005).

In field-scale applications, when quantifying oxygen transfer rates in whole tanks, the total oxygen transfer rate (OTR, $\text{kg}_{\text{O}_2}/\text{h}$) is expressed in terms of an apparent velocity of reaction and a driving force:

$$OTR = K_L a \cdot (c_\infty^* - c) \cdot V \quad (2.9)$$

where $K_L a$ is the apparent mass transfer coefficient. The difference between $k_L a$ and $K_L a$ is due to the difference in integration volumes for the two cases, a particular point into the aeration basin (as in the differential mass balance, eq. 2.1) and the whole aeration tank. In this work only $k_L a$ will be used.

2.1.3. Oxygen Absorption into Agitated Liquids

For the purpose of this study it is relevant to spend few more words about the effects of fluid motion on oxygen transfer. The more advanced interfacial theories are founded on the assumption of a non-stagnant fluid film (Higbie, 1935; Danckwerts, 1951, 1970), which in quantitative terms can be described as a distribution of ages for the surface volume elements (Danckwerts, 1951). Higbie's (1935) theory, also known as penetration theory, proposes a continuous regeneration of the surface with fresh fluid from the bulk. In his theory, the mass transfer coefficient will be expressed as:

$$k_L a \sim \sqrt{\mathcal{D} \cdot t_c} \quad \text{or} \quad k_L = 1.13 \cdot \sqrt{u_B D_{s,O_2} / d_B} \quad (2.10)$$

where t_c is the surface element contact time and k_L , u_B , and d_B are the velocity of adsorption, the interfacial gas-liquid velocity, and the bubble diameter, respectively.

A further refinement can be found in the model by Danckwerts (1951). In his description, the surface film elements will be no longer laminar, and their residence time will have a

normal distribution with surface age. The mass transfer coefficient will thus be dependent upon the surface rejuvenation rate, in the form of the surface element contact time r_c :

$$k_L a \sim \sqrt{D/r_c} \quad (2.11)$$

A higher degree of turbulence will therefore result in a higher mass transfer coefficient, as experience suggests. (see § 2.4). It should be noted that a shortcoming of these more complex models is the measurement and verification of the newly introduced variables, t_c and r_c ; this may result, for example, in the necessity for postulation of additional information, such as the surface age distribution (Danckwerts, 1970).

2.2. Bubble mechanics

There is a duality between bubbles and droplets, with few differences. Bubbles have higher buoyancy, therefore larger rising velocity. Also, mass transfer within the bubble will be larger since the gas diffusivity is larger than the liquid one. This results in a liquid controlling film system. Several times during the course of this review, both phenomenological descriptions for bubbles and droplets will be reported, since their similarity in behavior.

2.2.1. Dynamics of Bubble Formation

Studies on single bubbles are conducted with the generation of a bubble through an orifice at the bottom of a liquid container. At low gas flowrates (Sherwood et al., 1975):

$$d_b = \left(\frac{6d_o\sigma}{\Delta\rho \cdot g} \right)^{1/3} \quad (2.12)$$

where d_o = orifice diameter (L)

σ = equilibrium surface tension (F·L⁻¹)

$\Delta\rho$ = gas-liquid density difference (M·L⁻³)

Bubbles form in spherical shape, with higher frequency at higher flowrates, but with negligible variations in volume. At higher air flowrates bubbles will begin showing volumetric effects, i.e. bubble volumes will be significant to obtain deformations due to drag and buoyancy (Fan and Tsuchiya, 1990). Bubble shapes will then start to depart from the spherical shape, either reaching equilibrium at new shape regimes or breaking apart (Bhaga and Weber, 1981). This may result in a bubble size distribution (Danckwerts, 1970). Bubble shape can be described as a function of fluid characteristics and flow regime: Fig. 2.3 reports a map of shape regimes for single bubbles rising in a Newtonian fluid as function of the Reynolds, Morton and Eötvös dimensionless numbers. Remember that:

$$(\text{Re}) = \frac{d_b \cdot u}{\nu_l} \quad (2.13)$$

$$(\text{Eo}) = \frac{g \cdot d_b^2 \cdot \rho_l}{\sigma} \quad (2.14)$$

$$(\text{Mo}) = \frac{g \cdot \mu_l^4}{\rho_l \cdot \sigma^3} \quad (2.15)$$

where d_b = bubble equivalent diameter (= diameter of the volume-equivalent sphere)

μ_l = liquid dynamic viscosity

ν_l = liquid kinematic viscosity

ρ_l = liquid density

σ = surface tension

g = acceleration of gravity

u = bubble velocity.

In terms of physical significance, (Re) represents the ratio between inertial and viscous forces, (Eo) the ratio of gravity (or buoyancy) forces to surface tension forces, and (Mo) is the ratio of viscous forces to surface tension. A dimensional analysis based on these variables was first suggested by Haberman and Morton (1953). Introducing the Weber dimensionless number (Bhaga and Weber, 1981)

$$(\text{We}) = \frac{u^2 \cdot d_b \cdot \rho_l}{\sigma} = (\text{Re})^2 \cdot \sqrt{\frac{(\text{Mo})}{(\text{Eo})}} \quad (2.16)$$

the phenomenological description can be reduced to one group. This dimensionless number has been used by Moore (1959) to produce analytical solutions for the bubble

shape; these results provide a rather inaccurate estimate for a wide range of Weber numbers, in general for $(We) > 2$. Similar dimensional analyses have been applied in other studies (Zlokarnik, 1969, 1980a).

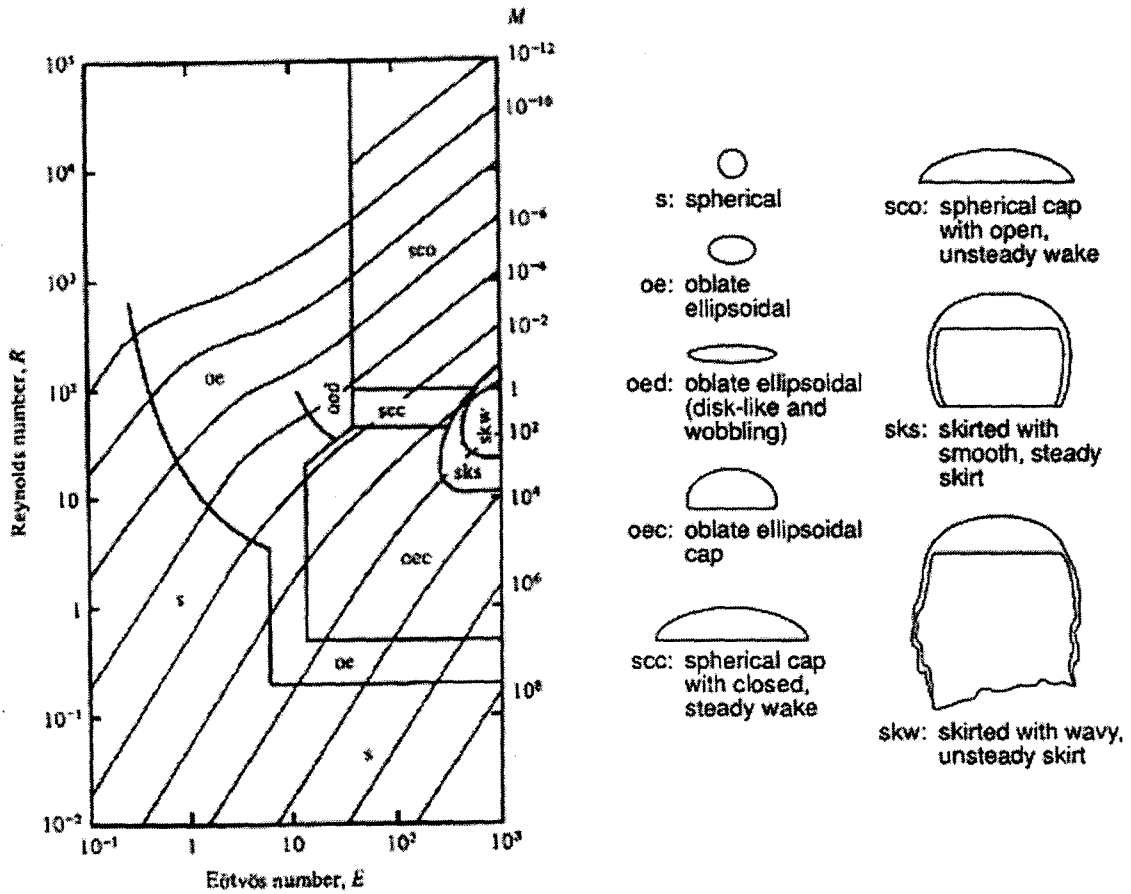


Figure 2.3. Map of single bubble shape regimes in a Newtonian fluid (after Bhaga and Weber, 1981). The key to the acronyms is presented aside (after Fan and Tsuchiya, 1990). In this figure R , E , and M are the Reynolds, Eötvös, and Morton numbers, respectively.

2.2.2. Surface Tension and its Measurements

Visual examples can easily describe the concept of surface tension: the rise of a liquid in a capillary tube, an insect “walking” on the water surface, or a polar liquid forming globules on a non-polar plastic surface. Formally, the surface tension is the work per unit distance required to expand the fluid interfacial area, or the minimum surface free energy. Both concepts are mathematically equivalent (Harkins, 1952).

Surface tension was first measured by Lecomte du Noüy (1919) with the ring method. Other investigators refined the method producing correction factors (Freud and Freud, 1930; Harkins and Jordan, 1930). This experiment consists in measuring the force required for detaching a wire ring horizontally laying in a liquid by pulling it out of the liquid along the direction normal to the ring area. Figure 2.4 illustrates the ring method.

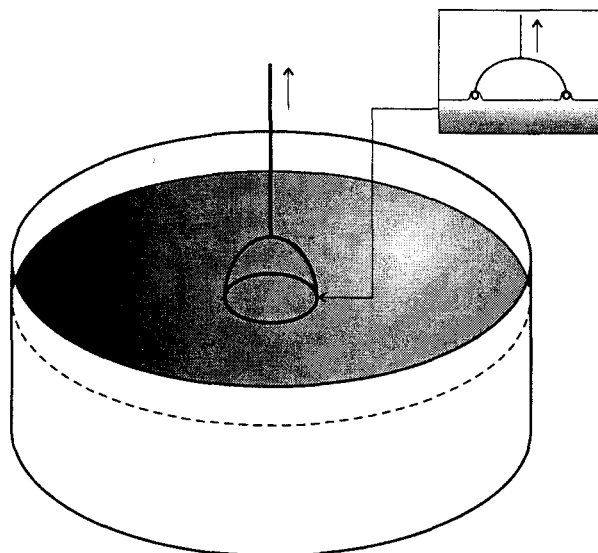


Figure 2.4. The du Noüy ring testing apparatus.

The molecular attraction between the two fluids dictates the extent of surface tension: it is of common sense that two immiscible fluids will minimize the interfacial area. This is due to the molecular attraction between molecules of the same fluid, which are attracted to one another more than to the other fluid's ones. In this fashion, the molecules at the surface will be characterized by a higher potential energy than the bulk, because it is at the interface that the molecules will feel net attraction from the backing bulk (Davis and Rideal, 1961).

The du Noüy method was designed to measure static surface tension, and although applications to surfactant solutions have been made (Lunkenheimer and Wante, 1981), other methods are specifically tailored for surfactant solution measurements, i.e. for the dynamic surface tension (DST) (Masutani, 1988). The earliest is the oscillating jet method (Bohr, 1909), which borrows geometrical considerations from wave theory (Savart, 1833; Rayleigh, 1879). When a pressurized liquid is forced through an elliptical orifice, a jet with properties of standing waves is formed. It can be visually observed that the jet offers periodical waves (Mancy and Barlage, 1968; Noskov, 1996). An advantage of this method is the detection at very low surface ages, as low as 0.001 s (Huo, 1998), while a remarkable drawback is that it cannot be used for long adsorption times ($t > 2s$) (Masutani, 1988).

By measuring the characteristics of a bubble (or a drop) forming at the end of a capillary tip it is possible to measure the surface tension during the drop formation: Pierson and Whitaker (1974) investigated the volumetric characteristics of a hanging drop during its

formation by a drop method, concluding that the stability of the drop was found to be dependent only on its shape. A major shortcoming of this method is the difficulty of determining the surface age (Masutani, 1988).

Sudgen (1922, 1924) assembled one of the first maximum bubble pressure measuring apparatus, which records the maximum pressure in a capillary or a maximum pressure difference between two capillaries of different radii, necessary to produce and detach a bubble from the capillary tip immersed in the liquid test solution. This method has the advantages of its measuring range and low costs (Masutani and Stenstrom, 1991).

Kloubek (1972a, 1972b) concluded after extensive studies that the bubble volume is independent of the depth of the capillary tip, and that its diameter increases linearly with the orifice diameter; also, the orientation of the capillary plays a role in the bubble detachment, and bubble volume and frequency are directly correlated.

Finally, factors that influence surface tension are temperature, viscosity, and the presence of electrolytes (Huo, 1998). Heat effects on the system are obvious since the analogy between thermal energy and work, the work necessary to increase the interfacial area. Secondly, surface tension appears higher in viscous fluids possibly because viscous forces oppose resistance to the displacement of fluid at the interface (Fainerman et al., 1993). The presence of electrolytes enhances the SAA effects on DST, while nonionic surfactants show no alteration (Burcik, 1950). The explanation lies in the reduction of surface-active potential due to free charges at interface, hence the decrease in resistance

to rapid adsorption (Huo, 1998). This effect was observed at long surface ages, rather than at surface formation (Burcik, 1950).

2.2.3. Internal Circulation Phenomena

Most of the description of bubble phenomena assume the analogy to solid spheres, since at very small diameters the growth of dynamic surface tension increases the drag coefficient to the value of rigid bodies (see §2.3.2 et §2.4.2) (Habermann and Morton, 1953). Despite this, it must be underlined that important effects are due to internal gas circulation (fig.2.5).

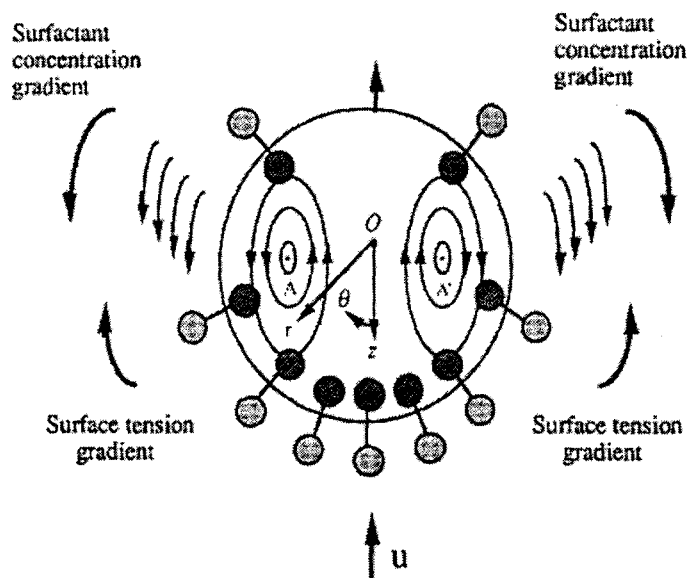


Figure 2.5. Internal bubble circulation and surface tension gradients (adapted from Edwards *et al.*, 1991). Note that surfactant molecules are here disproportionately represented. A, A' are the stagnation points.

Since the gas molecules at the bubble surface are not forced in their position by a solid lattice, they will be moved by the interfacial shear forces when in contact with the liquid, and they will cause themselves the movement of other inner gas molecules by gas-to-gas shear (Batchelor, 1967). This inner movement can be rigorously described as the rising of two adjacent vortices, hence inside the bubble there will be two stagnation points (Prandtl, 1934). At the same time, just outside the bubble the moving fluid can be described by streamlines tangent to the surface (Batchelor, 1967; Kunii and Levenspiel, 1969). The internal circulation, together with the external liquid-to-surface shear contributes to the accumulation of surfactants on the rear of the bubble, which is referred to as stagnant cap (Edwards et al., 1991; Vasconcelos et al., 2002). Evidence supports the existence of fore-and-aft symmetry in the concentration distribution at the interface (Clift et al., 1978; Ramirez and Davis, 1999). Coarse-bubbles are characterized by a zone usually referred to as wake, which is caused by the instability in water of air bubbles larger than 10mm.

Since the asymmetry of the surface concentration, studies were conducted to evaluate the mass transfer coefficient as a function of the angular position on the surface (Ramirez and Davis, 1999). Despite these arguments, Rodrigue et al. (1996) concluded that in the case of small bubbles in surfactant solutions, the SAA effects in internal circulation will be such that bubbles can be assimilated to solid spheres following Stokes' law. By covering part of the bubble surface, surfactants increase surface rigidity, and the bubble drag coefficient increases approaching that of a rigid sphere, resulting in a diminished terminal velocity (Haberman and Morton, 1953; Alves et al., 2005).

An issue that needs to be raised here is the discussion on the internal gas depletion. It is intuitive that a tiny air bubble rising in a tank will experience oxygen depletion after a certain travel time. This will be reflected in a lower concentration gradient, therefrom a lower mass transfer. While having lower concentration gradient, the bubble will experience a reduction in mass, compensated by an expansion due to reduced liquid pressure with rise. The comparison of the two effects is not clear yet, although Vasconcelos et al. (2002) concluded that the diameter of the bubble decreases linearly with time, at a rate proportional to the mass transfer coefficient. All the available oxygen transfer models shortcut the discussion assuming that the gas-phase oxygen concentration does not vary over time (pseudo-steady-state assumption) (Carver, 1969; ASCE, 1984, 1991, 1997; Chern and Yu, 1997; Chern et al., 2001; Vasconcelos et al., 2002). Despite this, Motarjemi and Jameson (1978) reported experiments that show that fine bubbles ($d_b < 2$ mm) of pure oxygen transfer about 2/3 of their mass when rising in a 4 m-deep column of water.

2.2.4. Bubble - Bubble Interactions

Bubble coalescing phenomena have been a matter of study since bubbles started to be exploited in chemical engineering (Marucci and Nicodemo, 1967; Kunii and Levenspiel, 1969). The payback of investigating these phenomena has been the evolution of more coalescence inhibiting systems, which offer more efficient gas transfer (Zlokarnik, 1978a, 1980b). In a pure liquid, bubbles coalesce as soon as they move afar from a high shear liquid region, and form larger bubbles, thus lowering specific transfer areas and times

(Zlokarnik, 1978a). Zlokarnik (1978a, 1978b, 1979, 1980b) extensively explored coalescence, and described pure liquids as favoring coalescing conditions, while contaminated solutions in general as coalescing inhibiting systems. This is because surfactant solutions experience SAA surface accumulation, which results in the formation of a film between adjacent bubbles; the energetic cost for breaking this film prevents coalescence, thus allowing the existence of smaller bubbles and foam (Zlokarnik, 1978a). Further explanations on surface accumulation concepts will be offered in §2.3.2. It is possible to quantify the degree of coalescence by selecting the salt addition, and experiments for this purpose have been done (see §2.4.3) (Zlokarnik, 1979, 1980b).

Antifoaming agents are used in very low concentrations to enhance coalescence (Libra, 1993). Zlokarnik (1980b) reported that nonionic surfactants may serve this purpose. The available oxygen transfer models, although being developed for clean water with no bacterial floc, neglect coalescence effects (ASCE, 1984, 1991, 1997; McGinnis and Little, 2002). For the datasets analyzed in this study, the assumption of negligible coalescence largely adopted in previous mass transfer models was adopted.

2.3. Surface Active Agents

2.3.1. Classification and Properties

During the last half century the chemical industry engineered compounds tailored to reduce surface tension, which are usually referred to as surface active agents (SAA).

They occur in the most common form of a polar head and a hydrocarbon (non-polar) tail (Fig.2.6) (Tadros, 1984).

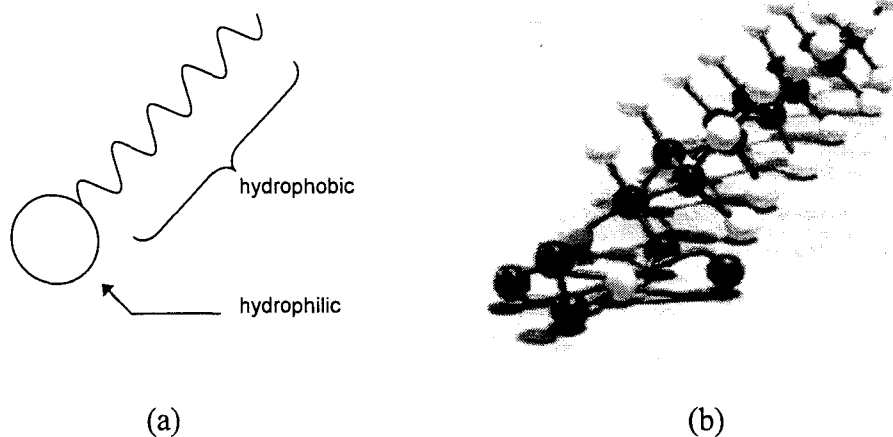


Figure 2.6. Schematic drawing (a) of a surface active agent molecule and (b) molecular model of sodium lauryl sulfate (after Fujimoto, 1985).

Depending on the nature of the head-group, SAA are classified as anionic, cationic, nonionic and zwitterionic (Rosen, 1978; Thadros, 1984). For brevity, only the chemical description of the surfactants employed in this study will be given. When present in aqueous solution, the non-polar tails of surfactant molecules experience repulsion with (polar) water molecules, therefore they try to reach an equilibrium state by reducing the interfacial area between water and tails to a minimum (Fig. 2.7a), and by pushing the tails into the gas media (Fig. 2.7b) (Fujimoto, 1985).

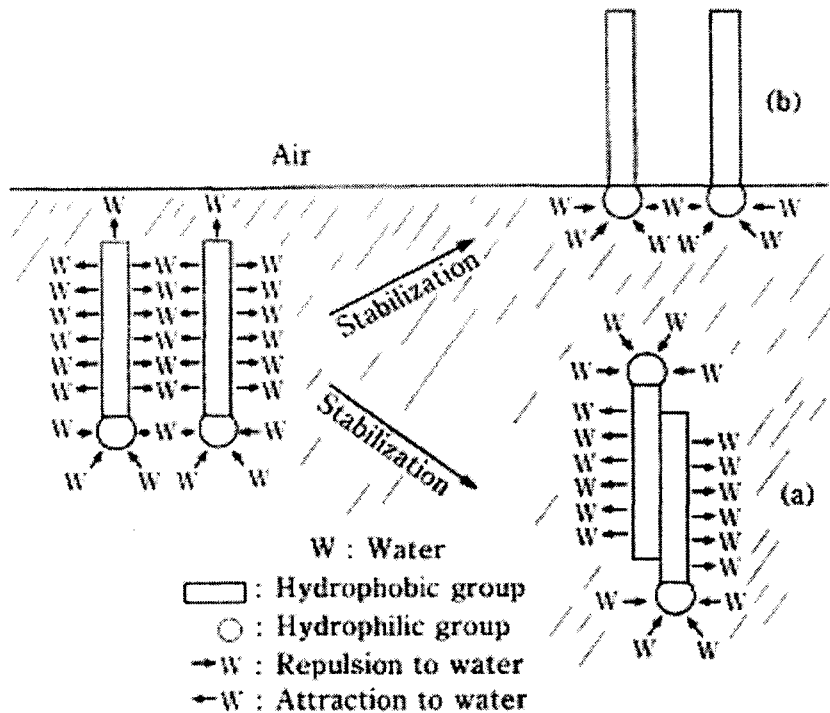


Figure 2.7. The two ways of SAA molecular stabilization (Fujimoto, 1985)

The diffusional velocity of molecules migration depends on their molecular volume (Bird et al., 1960). Therefrom, higher molecular weight SAA can be referred to as slow surfactants, whilst it is customary to refer to lower molecular weight compounds as fast surfactants (Ferri and Stebe, 2000).

2.3.2. Liquid Side: Adsorption at Gas - Liquid Interfaces

Since the minimization of tail-to-water contact area, surfactants adsorb at gas-liquid interfaces in a regularly distribute, usually charged, monolayer, which reaches its maximum thickness at the critical micelle concentration (CMC) (Rosen, 1978). The

interface will appear more rigid by virtue of the presence of the monolayer, which stabilizes it (Masutani and Stenstrom, 1991). Fig. 2.8 shows the surface monolayer at both bubble-to-liquid and liquid-to-air interfaces: the bubble stabilization due to the surfactant allows gas bubbles to exist at the top of the liquid, a common example being seawater foam.

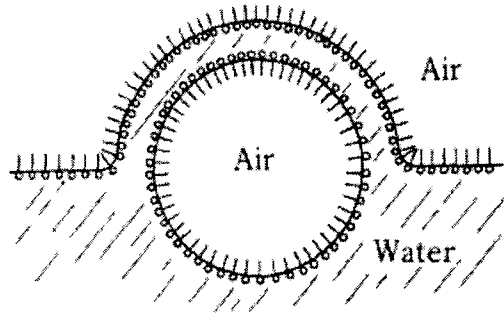


Figure 2.8. Interfacial monolayer and foaming effect (Fujimoto, 1985)

The minimum surface tension will be reached at CMC, thus any SAA concentration above CMC will not result in any decrease in surface tension (Caskey and Barlage, 1971). In case of SAA concentrations beyond CMC, a multilayer will form at the interface (Mancy and Okun, 1960).

For diffusion-controlled adsorption a Langmuir isotherm is suitable to relate dynamic surface tension $\gamma(t)$ ($\text{N}\cdot\text{m}^{-1}$), solvent surface tension γ_0 ($\text{N}\cdot\text{m}^{-1}$), and dynamic interfacial adsorption (or surface accumulation) $\Gamma(t)$ ($\text{mol}\cdot\text{m}^{-2}$):

$$\gamma(t) = \gamma_o + RT \cdot \Gamma_\infty \cdot \ln \left[1 - \frac{\Gamma(t)}{\Gamma_\infty} \right] \quad (2.17)$$

where Γ_∞ is the limiting surface accumulation at equilibrium ($\text{mol} \cdot \text{m}^{-2}$), R the universal gas constant ($\text{J} \cdot \text{mol}^{-1} \cdot \text{K}^{-1}$) and T the absolute temperature (K). Expanding the logarithm in eq.2.17 into a series and truncating after the first term we obtain the approximation of eq.2.17 for early stages:

$$\gamma(t) = \gamma_o - RT \cdot \Gamma(t) \quad (2.18)$$

Eq.2.18 can be solved for $\Gamma(t)$, when γ_o and $\gamma(t)$ are known:

$$\Gamma(t) = \frac{\gamma_o - \gamma(t)}{RT} \quad (2.19)$$

The dynamic interfacial accumulation $\Gamma(t)$ approaches the equilibrium value Γ_∞ at the very long bubble age limit. This occurs in the long time limit because surface contaminants concentration has reached a constant value. This also causes the dynamic surface tension to approach a minimum, constant value. The equilibrium surface accumulation can be extrapolated from $\Gamma(t)$ patterns at long-time limits, as well as calculated from the Gibbs equation (for a surfactant solution of concentration c_B)

$$\Gamma_\infty = -\frac{1}{RT} \frac{d\gamma}{d \ln c_B} \quad (2.20)$$

which treats adsorption as a thermodynamic process. The ratio $d\gamma/d\ln c_B$ can be calculated from the slope of the semi-logarithmic surfactant characteristic curve (Fainerman et al., 1994), such as the curve represented in Fig.2.9, which relates equilibrium surface tension to the surfactant bulk concentration (see chapter 4).

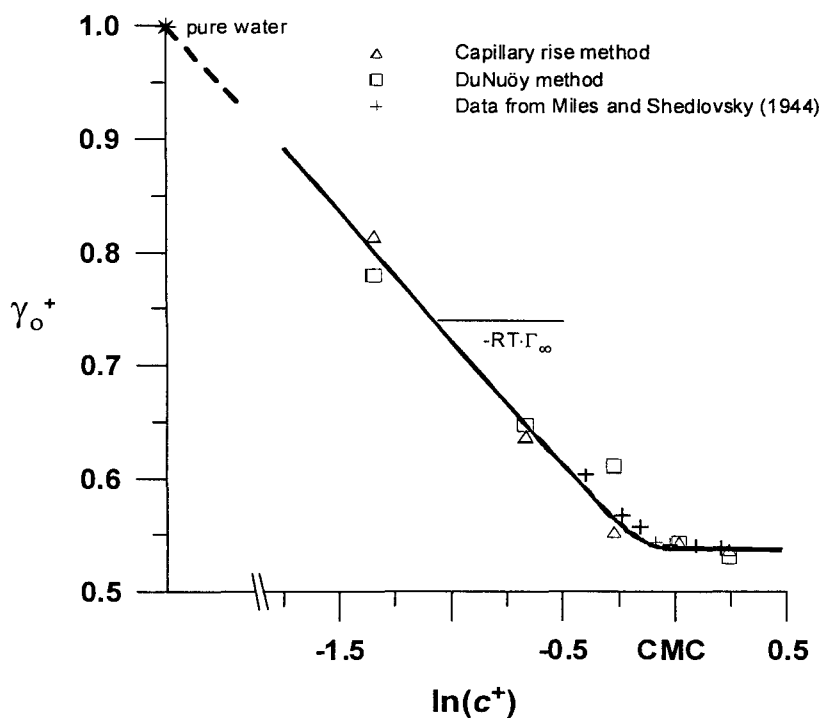


Figure 2.9. Dimensionless characteristic curve for sodium dodecyl sulfate solutions (Huo, 1998). The horizontal axis is the natural logarithm of the dimensionless concentration $c^+ = c_B/CMC$.

The time-dependent diffusion-controlled dynamic interfacial adsorption kinetics at air-aqueous surfactant solutions was first quantified with an analytical equation by Ward and

Tordai (1946). Their equation relates surfactant interfacial accumulation $\Gamma(t)$ with surfactant interfacial concentration and diffusivity for planar surfaces, accounting for surfactant back-movement to the subsurface (in the integral term). The Ward and Tordai equation can be written in spherical coordinates by solving the diffusion equation

$$\frac{\partial c}{\partial t} = \nabla \cdot \mathcal{D}_{SAA} \nabla c \quad (2.21)$$

between the bubble surface and the subsurface, following the boundary considerations of constant bulk concentration at infinite distance from the interface, initial concentration equal to bulk, and concentration at subsurface equal to subsurface concentration $\phi(t)$ (Liu et al., 2004). The subsurface is defined as the surface of the spherical region outside the semi-spherical forming bubble with diameter equal to the capillary. Figure 2.10 illustrates the integration domain.

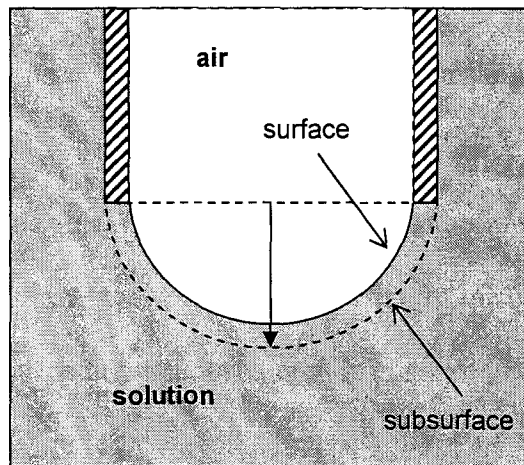


Figure 2.10. Integration domain for a forming bubble (Liu et al., 2004).

The outer integration limit, the bubble subsurface, is the point at which the bubble will have maximum pressure, corresponding to the bubble having diameter equal to the capillary diameter. By neglecting the diffusivity gradient within the integration domain, equation 6 can be solved as (Ward and Tordai, 1946; Liu et al., 2004):

$$\Gamma(t) = \frac{\mathcal{D}_s \cdot c_B \cdot t}{r_o} - \frac{\mathcal{D}_s}{r_o} \cdot \int_0^t \phi(t) dt + 2 \left(\frac{\mathcal{D}_s}{\pi} \right)^{1/2} \cdot \left\{ c_B \cdot t^{1/2} - \int_0^{t^{1/2}} \phi(z) d[(t-z)^{1/2}] \right\} \quad (2.22)$$

where c_B = bulk concentration ($M \cdot L^{-3}$)

$\phi(t)$ = subsurface concentration ($M \cdot L^{-3}$)

\mathcal{D}_s = surface diffusivity ($L^2 \cdot T^{-1}$)

r_o = initial bubble radius or the orifice radius (L)

There are numerous proposed simplifications of eq.2.22 for the short- and long-time adsorption cases (Hansen, 1960; Rillaerts and Joos, 1982; Daniel and Berg, 2001, 2003).

The short-time behavior is obtained by assuming a net migration of surfactants to the bubble, i.e. neglecting the integral terms which account for the backwards movement of solute. At short-time adsorption limits it is therefore possible to calculate the surfactant interfacial accumulation $\Gamma(t)$ by solving the truncated Ward and Tordai equation in spherical coordinates (Liu et al., 2004):

$$\Gamma(t) = \frac{\mathcal{D}_{SAA} \cdot c_B \cdot t}{r_o} + 2c_B \left(\frac{\mathcal{D}_{SAA} \cdot t}{\pi} \right)^{1/2} \quad (2.23)$$

The equation for long-time behavior is derived by either expanding the integral at long times (Hansen limit; Hansen, 1960), or neglecting the change in interfacial surfactant concentration at long times, which allows it to be factored outside the integral (Joos limit; Rillaerts and Joos, 1982). Daniel and Berg (2001) analyzed diffusion coefficients calculated with both the Hansen and Joos equations, and concluded that only the Hansen limit describes surface behavior at long-time limits. The Hansen point-to-point limit equation is a rearrangement of the approximated Ward and Tordai equation and can be used to calculate interfacial diffusion coefficients:

$$\mathcal{D}_{s,SAA} \rightarrow \frac{1}{\pi \cdot t} \left(\frac{\Gamma(t)}{c_B} \right)^2 \quad (2.24)$$

Therefore, substituting (2.19) into (2.24) we can calculate the surface diffusivity as a function of the dynamic surface tension:

$$\mathcal{D}_{s,SAA} \rightarrow \frac{1}{\pi \cdot t} \left(\frac{\gamma_o - \gamma(t)}{c_B \cdot RT} \right)^2 \quad (2.25)$$

In cases of surfaces moving at high shear rates in highly contaminated liquids or with interfacial temperature gradients, surface concentration gradients are established, leading to counterflow interfacial liquid circulation, known as the Marangoni effect, named after its first observer (Marangoni, 1871; 1872). The effect consists in a net movement of fluid

at interface due to the interfacial tension gradient. The tension gradient itself is a product of the inhomogeneous distribution of SAA on the surface, i.e. a concentration gradient (Edwards et al., 1991). Marangoni effects have significant effect in process involving high temperature or interfacial shear gradients, such as boiling contaminated liquids (Wasekar and Manglik, 2003). The Marangoni effects can be quantified by calculating the Marangoni dimensionless number:

$$(\text{Ma}) = \frac{R \cdot T \cdot \Gamma_o}{u \cdot \mu} \quad \text{or} \quad (\text{Ma}) = \frac{\Delta\gamma \cdot r}{\mathcal{D} \cdot \mu} \quad (2.26)$$

where R = universal gas constant (8.314 J/mol·K)

T = absolute temperature

Γ_o = interfacial accumulation ($\text{m} \cdot \text{L}^{-2}$)

u = interfacial velocity ($\text{L} \cdot \text{T}^{-1}$)

μ = dynamic viscosity ($\text{M} \cdot \text{L}^{-1} \cdot \text{T}^{-1}$)

$\Delta\gamma$ = differential surface tension ($\text{F} \cdot \text{L}^{-1}$)

r = characteristic length (L)

\mathcal{D} = interfacial diffusivity ($\text{M} \cdot \text{L}^{-2}$)

The Marangoni numbers for the datasets used in this study were calculated and were below 1. Therefore, in this study Marangoni effects were neglected.

2.3.3. Gas Side: Effects on Oxygen Transfer

The earliest observations of gas transfer depression caused by solutes can be traced back to the earliest developments in activated sludge operation (Kessener and Ribbius, 1934). Mancy and Barlage (1968) hypothesized that SAA inhibit oxygen transfer by obstructing the molecular diffusion of oxygen molecules through the interfacial barrier, and the SAA physiochemical characteristics will play a role in this. This theory will be later discussed and criticized in the results and discussion section (chapter 4). Davis (1972, 1977) suggests that SAA increase the thickness of the surface layer to be displaced by turbulent eddies, thus depressing mass transfer. It has also been observed that SAA decrease surface renewal rates (Eckenfelder et al., 1956) and increase interfacial viscosity (Mancy and Okun, 1960). Higher molecular weight surfactants show retardation in the oxygen transfer inhibition, due to diffusional time requirements (Masutani and Stenstrom, 1991).

Eckenfelder observed mass transfer coefficient depression in fine- and coarse- bubble aeration systems (Eckenfelder, 1959). Eckenfelder and Barnhart (1961) reported the effects of organic substances on mass transfer, showing that contamination as low as 15 mg/l of sodium lauryl sulphate can reduce mass transfer coefficients to 0.5 times the value in clean water. Figure 2.11 shows the decrease in magnitude for volumetric mass transfer coefficients ($k_L a$) and velocity of adsorption (k_L) with increasing contamination. Note that $k_L a$ recovers at higher contamination. This phenomenon is due to the stability of smaller bubbles at higher contamination, hence to a favored interfacial specific area.

The mass transfer recovery is nevertheless small, if compared to the initial value in pure water.

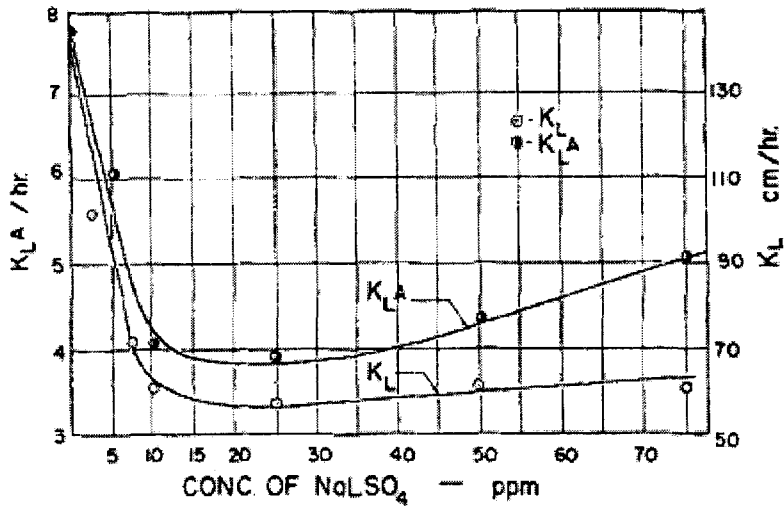


Figure 2.11. Volumetric mass transfer coefficient ($k_L a$) and velocity of adsorption (k_L) in solutions with various concentrations of sodium lauryl sulfate (Eckenfelder and Ford, 1961).

Mass transfer is favored for smaller radii, since specific areas are higher, and the contact time is larger due to smaller buoyancy. Since SAA stabilize smaller bubbles, they should favor mass transfer. Also, SAA might prevent bubbles from coalescing, which favors the specific interfacial area (Zlokarnik, 1978a, 1979, 1980b). These beneficial effects are although overcome by causes attributed to the surface diffusional obstruction (Springer and Pigford, 1970) and by hydrodynamic obstruction to surface renewal due to the

Marangoni effect (Llorens et al., 1988), with a net observed effect of oxygen transfer depression (Masutani and Stenstrom, 1991).

A proposed approach for modeling surface contamination is the stagnant cap model (Griffith, 1960). In case of fast surface convection, it can be assumed that all the surfactant accumulates on the stagnant rear cap of the bubble, leaving the frontal region virtually free of contamination (Vasconcelos et al., 2002; De Kee and Chhabra, 2002). This approach has been applied to model experimental data, integrating the balance that describes the surface cap evolution, with an integration constant evaluated from fitting the data (Vasconcelos et al., 2002).

Static surface tension effects on oxygen transfer have been investigated, but with no correlation (Stenstrom and Gilbert, 1981; Wagner and Pöpel, 1996). Dynamic surface tension measurements, instead, showed to be correlated to the mass transfer coefficient in several experiments (Masutani, 1988; Huo, 1998). A discussion on the experimental evidence will be presented in §2.4.

The interfacial surfactant accumulation is a time-dependent phenomenon shown by the evolution over time of the interfacial tension, in this case defined dynamic surface tension (DST). Surfactant accumulation at contaminated bubble interfaces is characterized by the accumulation of hydrophilic heads at the gas-liquid interface, and the arrangement of the hydrophobic tails inside the bubble volume, occurring by chemical exclusion (Rosen, 1978). This results in increased drag coefficients and, furthermore, the presence of hydrophobic tails inside the bubble reduces the internal gas circulation, which reduces

renewal of the gas-side mass-transfer film (Garner and Hammerton, 1954). Boussinesq (1913) first proposed that the reduction in internal gas circulation in bubbles and drops is due to the interfacial accumulation of contaminants organized as a monolayer, which was validated experimentally by Garner and Hammerton (1954).

The interfacial shear generated by the rising bubble causes the accumulation of surfactants on the lower bubble region, also called stagnant-cap. Evidence supports the existence of fore-and-aft symmetry in the interfacial concentration field (Clift et al., 1978; Fan and Tsuchiya, 1990). Several mass transfer models utilized the stagnant-cap hypothesis with success (Griffith, 1960; Weber, 1975; Sadhal and Johnston, 1983; Vasconcelos et al., 2002).

2.4. Experimental Observations

There are several experimental observations of the aforementioned phenomena, and they will be catalogued and presented in this section. For brevity, the references will be cited in each of the following paragraphs only.

2.4.1. Effects on Dynamic Surface Tension

- As described previously, the higher the SAA concentration, the lower the surface tension, with exponential decay (fig.2.12). This has been reported in several observations in the form of static surface tension vs. SAA concentration (e.g.: Hwang and Stenstrom, 1979; Masutani, 1988; Libra, 1993; Huo, 1998; Ferri and Stebe, 2000).

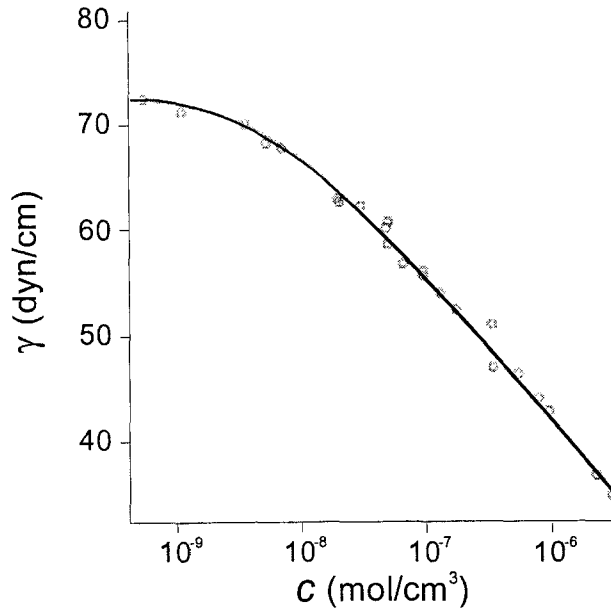


Figure 2.12. Surface tension of Surfynol 104 solutions as a function of SAA additions. The solid line represents a Langmuir model prediction (adapted from Ferri and Stebe, 2000).

When dealing with bubbles across their whole lifespan, it is more significant to measure the dynamic surface tension (fig.2.13). This was repeated in several occasions (Mancy and Barlage, 1968; Masutani, 1988; Masutani and Stenstrom, 1991; Chang and Franses, 1994; Noskov, 1996; Huo, 1998; Lee, 2003). It must be noted from fig.2.13 that the slower surfactant (Tergitol) depresses the DST over a longer time-scale (remember the discussion in §2.3.1). This sustains the need to account for SAA diffusional effects.

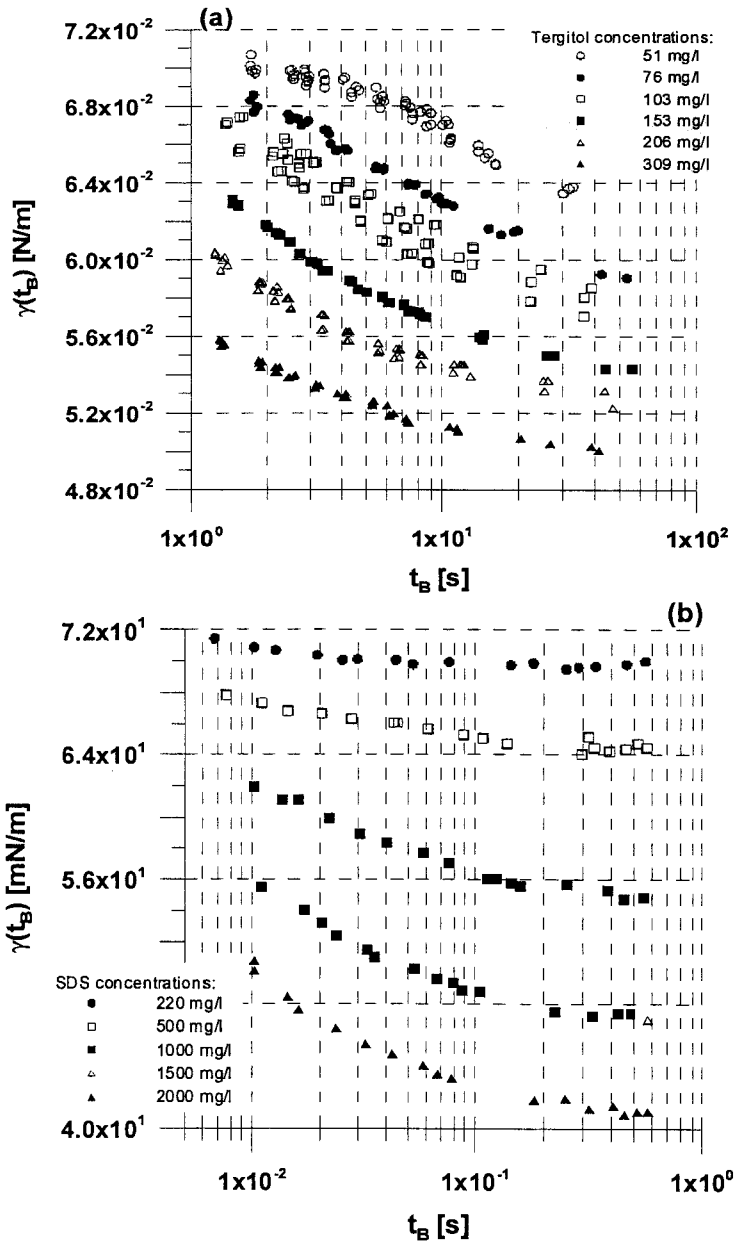


Figure 2.13. Dynamic surface tension of Tergitol (a) and sodium dodecyl sulfate (b) solutions. Note the different time scales for similar surfactant concentrations: compare 220 mgSDS/l vs. 309 mgTergitol/l, since $MW_{\text{SDS}} = 288$ and $MW_{\text{Tergitol}} = 316$ a.m.u. (adapted from: (a) Masutani, 1988; (b) Huo, 1998).

2.4.2. Effects on Terminal Velocity

The effects on terminal velocity are described in classic work by Habermann and Morton (1953). Several other experiments were performed by others, all confirming their results (e.g., Calderbank et al., 1970; Motarjemi and Jameson, 1978; De Kee and Chhabra, 2002; McGinnis and Little, 2002). Fig.2.14 reports the results, which include plots for both pure and contaminated water.

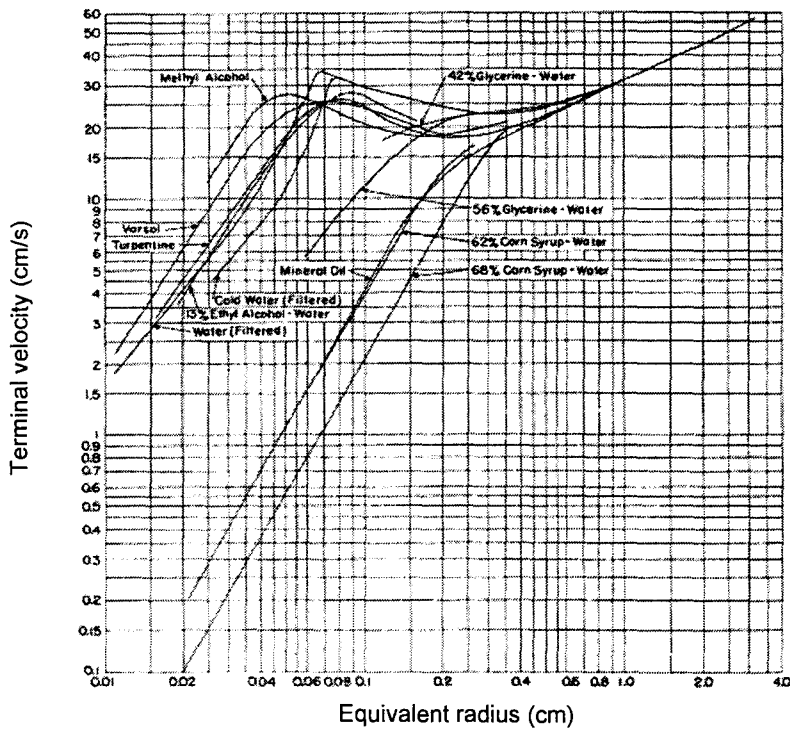


Figure 2.14. Terminal velocities for air bubbles in filtered water and contaminated liquids (adapted from Habermann and Morton, 1953).

The effects of commercial surfactants on the drag coefficient are reported in fig. 2.15.

Note the assimilability between rigid spheres and gas bubbles at low Reynolds' numbers (see §2.2.3).

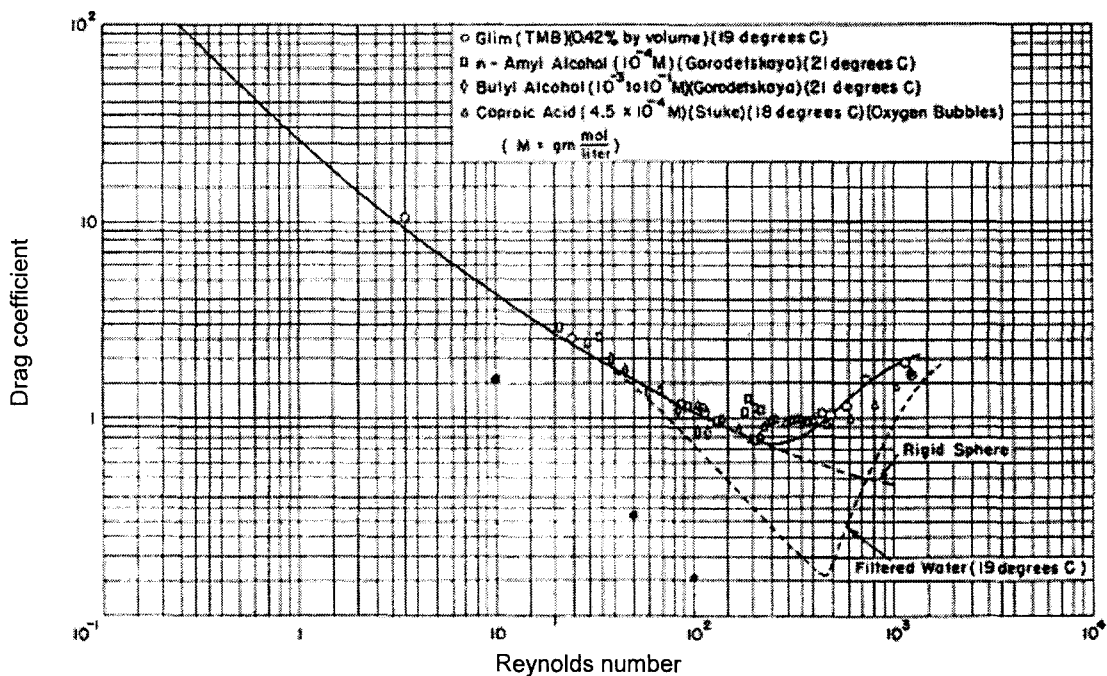


Figure 2.15. Drag coefficient for air bubbles as a function of the Reynolds number in filtered water and surfactant solutions (adapted from Habermann and Morton, 1953).

2.4.3. Effects on the Mass Transfer Coefficient

The first observations on mass transfer coefficient depressions in presence of contamination were reported by Kessener and Ribbius (1934). Several investigators graphed the depression of the mass transfer coefficient (or its ratio to the one in clean

water, i.e. α) versus SAA dosing and DST (Zlokarnik, 1978a, 1978b, 1979, 1980b; Masutani, 1988; Masutani and Stenstrom, 1991; Huo, 1998; Chindanonda, 2002; Lee, 2003). Calderbank et al. (1970) extended the measurements to bubbles of several centimeters, in both pure and contaminated water. The plots that will be here reported are the most significant to visualize the goal of the study explained in the following chapter.

First, the effects of salts and alcohols dosage on the alpha factor are shown in fig.2.16. It is clear that they act as mass transfer enhancers.

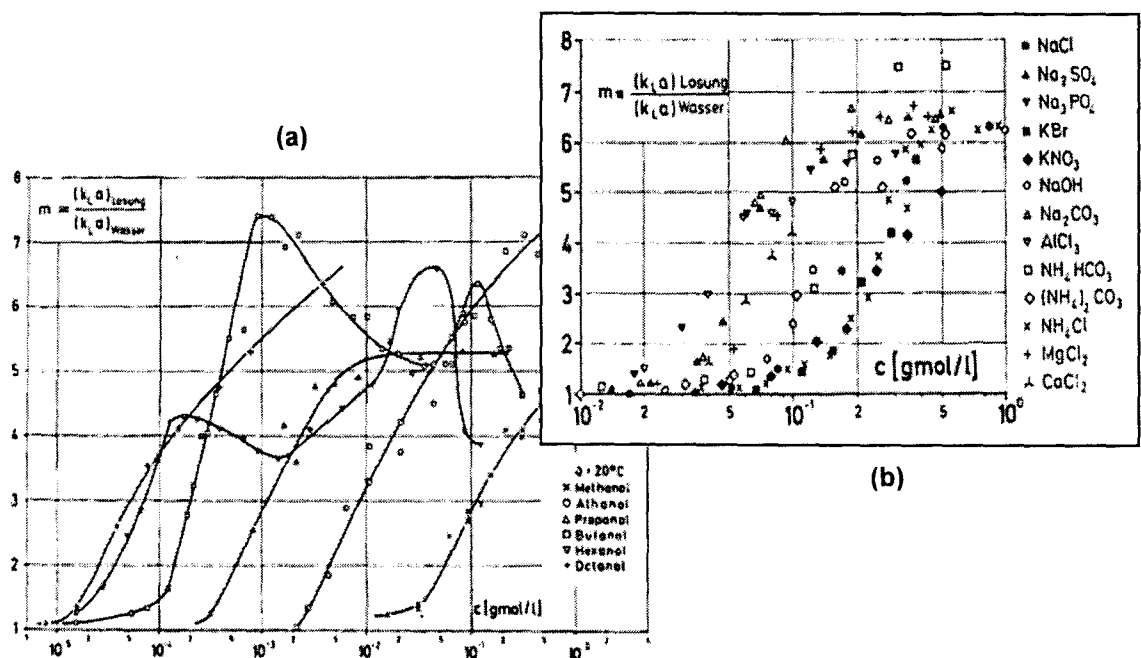


Figure 2.16. Mass transfer effects: enhancement by salts (a) and aliphatic alcohols (b). Note that here $m = \alpha$ (after Zlokarnik, 1980b).

Note that higher mass transfer coefficient does not necessarily produce higher oxygen transfer. In the case of sea water, for example, the mass transfer coefficient is higher, but the DO concentration at saturation is lower, to an extent that their product results in overall lower mass transfer rates.

Secondly, a similar plot is proposed (fig.2.17), but using commercial antifoam agents, which favors bubble coalescence (a), and commercial SAA (b). Note that the concentration scales for figs.2.16 and 2.17 are different by orders of magnitude.

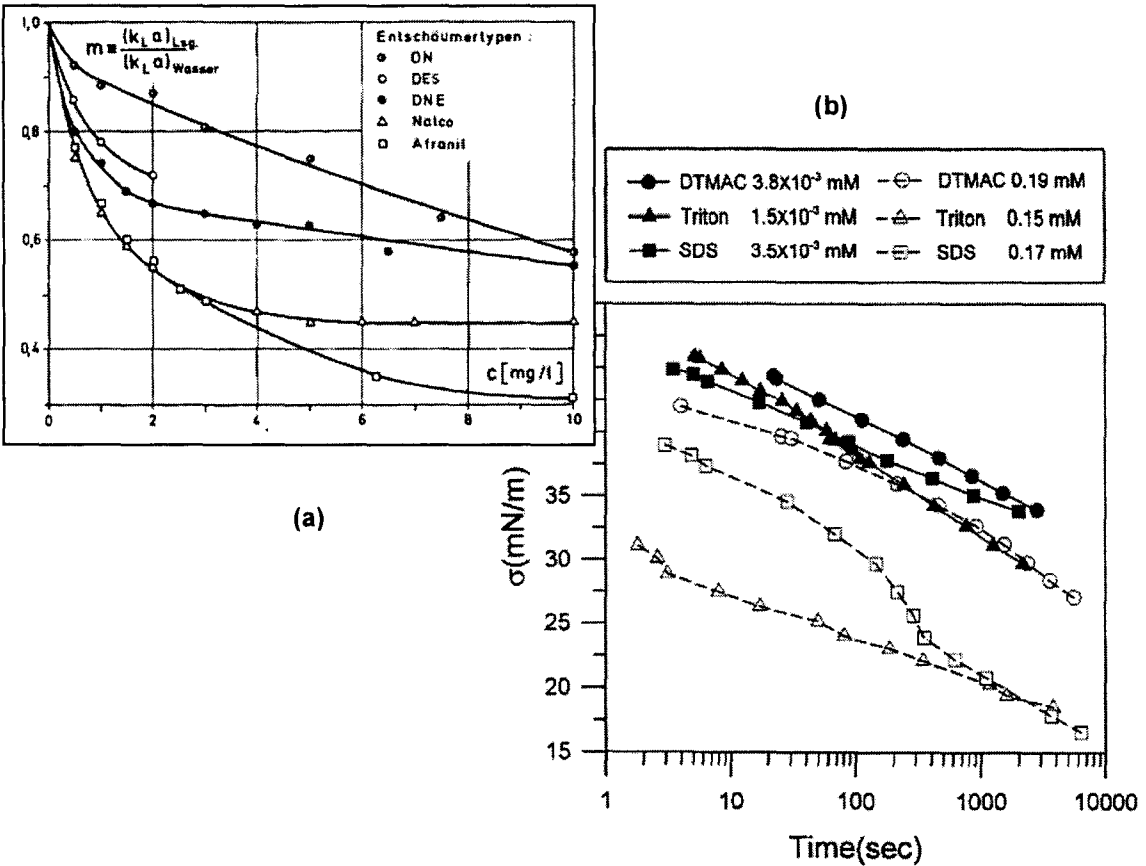
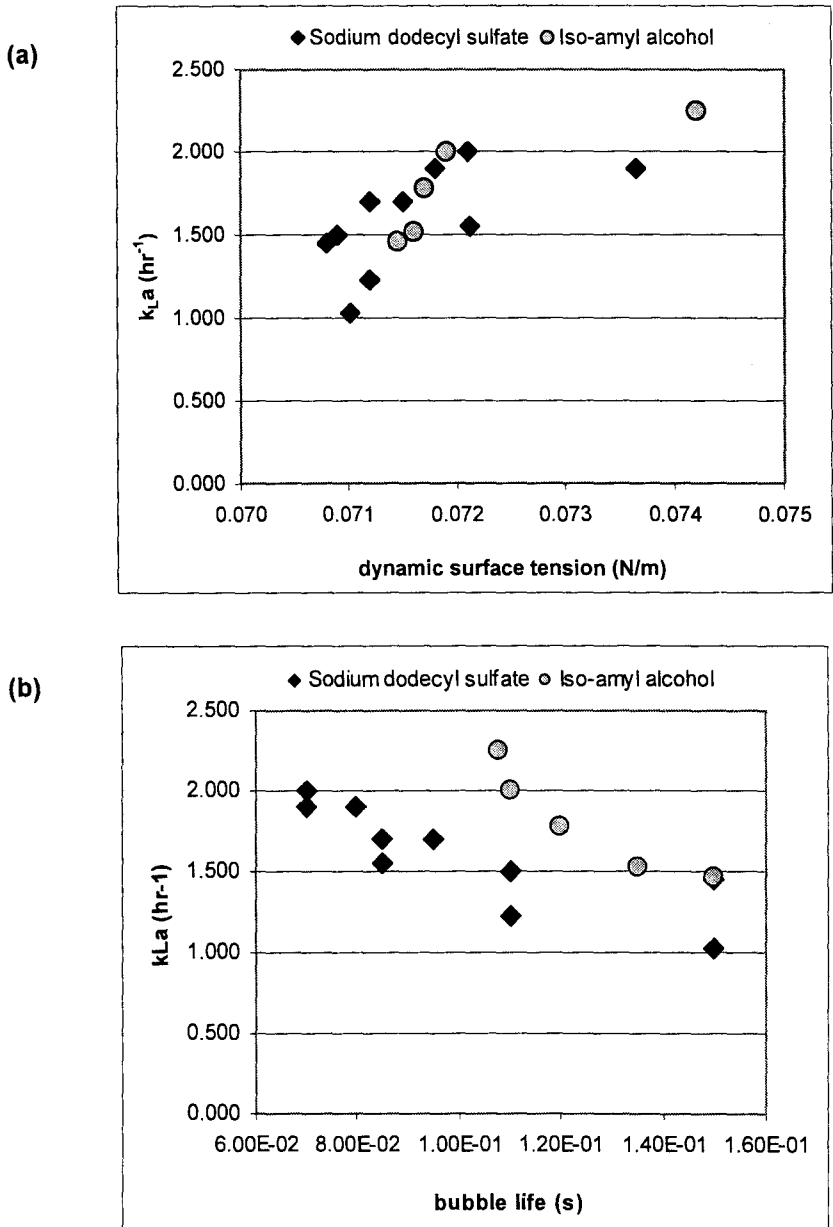


Figure 2.17. Mass transfer effects: depression by antifoam agents (a) and by surfactants (b) (after: (a) Zlokarnik, 1979; (b) Lee, 2003).

Finally, the depression of mass transfer over time (bubble age) is shown in fig.2.18a.

Using DST measurement over the same scale it is possible to graph mass transfer coefficient versus dynamic surface tension (fig.2.18b). The direct correlation between the two is unequivocal. Fig.2.18c confirms this with different experiments.



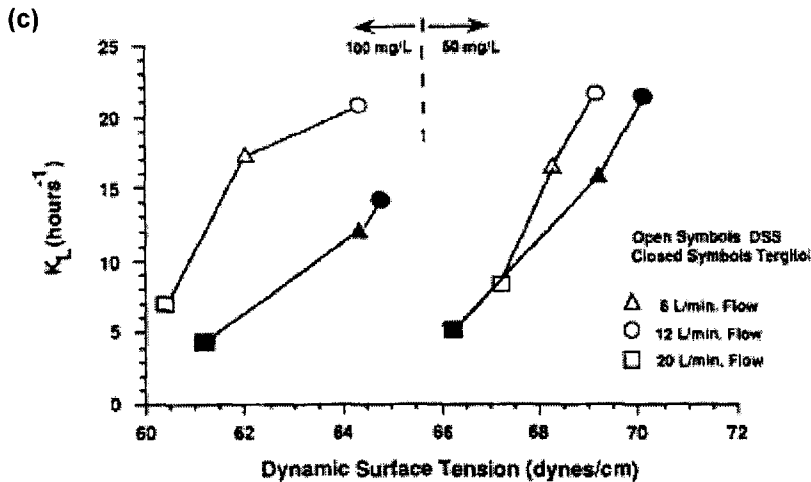


Figure 2.18. Mass transfer effects: effects on the mass transfer coefficient [(a,b) adapted from Huo, 1998; (c) after Masutani and Stenstrom, 1991].

2.5. Summary

The available literature offers theoretical tools and experimental results useful to this research. Models that describe oxygen transfer under several assumptions were developed. More refined mass transfer models allow corrections to more realistic scenarios, although introducing variables difficult to measure. Bubble formation and dynamics have also been studied by dimensional analysis. Several phenomena occurring inside the bubble, at its interface, and outside have been described, quantified, and observed. The chemistry of SAA has been extensively investigated, and their properties in solution abundantly observed. SAA effects on physical parameters have been experimentally observed, including effects on DST, terminal velocity, time-dependent

interfacial accumulation, and mass transfer coefficient. No comprehensive study including the dependence of interfacial properties on the surfactant concentration and nature is available yet. Table 1 summarizes the sources presented in this chapter.

Table 2.1. Summary of available literature sources.

THEORY / EXPERIMENT	AVAILABILITY	REFERENCE
steady-state G-L transfer model	YES	Lewis and Whitman (1924) Stenstrom and Gilbert (1981) ASCE (1984, 1991, 1997) Chern and Yu (1997) Chern <i>et al.</i> (2001)
unsteady-state G-L transfer model	YES	Higbie (1935) Danckwerts (1951, 1970) Vasconcelos <i>et al.</i> (2002) De Kee and Chhabra (2002)
unsteady-state G-L transfer observations	YES	Danckwerts (1951) Ramirez and Davis (1999)
mass transfer predictions: solid spheres in clean water	YES	Friedlander (1957, 1961)
mass transfer observations: solid spheres in clean water	YES	Boussinesq (1913) Frössling (1938) Griffith (1960) Johnson <i>et al.</i> (1967) Motarjemi and Jameson (1978)
mass transfer predictions: bubbles in clean water	YES	Higbie (1935) Friedlander (1957, 1961)
mass transfer observations: bubbles in clean water	YES	Stenstrom and Gilbert (1981) Capela <i>et al.</i> (2001) McGinnis and Little (2002)
mass transfer predictions: bubbles in contaminated water	NO	-
mass transfer observations: bubbles in contaminated water	YES	Ward and Tordai (1946) Hansen (1960) Mancy and Okun (1960) Eckenfelder and Ford (1968) Mancy and Barlage (1968) Carver (1969) Zlokarnik (1977, 1978a, 1979) Rillaerts and Joos (1982) Llorens <i>et al.</i> (1988) Masutani (1988) Masutani and Stenstrom (1991) Huo (1998) Chinanonda (2002)

THEORY / EXPERIMENT	AVAILABILITY	REFERENCE
dimensional analyses	YES	Moore (1959) Zlokarnik (1969, 1980a, 2002) Hwang and Stenstrom (1979) Bhaga and Weber (1981) Liger-Belair (2003)
surfactant chemistry	YES	Rosen (1978) Tadros (1984) Fujimoto (1985)
surface tension measuring methods	YES	Bohr (1909) Lecomte du Noüy (1919) Sudgen (1922, 1924) Freud (1930) Harkins and Jordan (1930) Caskey and Barlage (1971) Kloubek (1972a, b) Pierson and Whitaker (1976) Feinerman <i>et al.</i> (1994)
static surface tension measurements: contaminated water	YES	Hwang and Stenstrom (1979) Masutani (1988) Libra (1993) Chang and Franses (1994) Wagner and Pöpel (1996) Huo (1998)
dynamic surface tension modeling: contaminated water	YES	Levich (1959, 1962) Crooks <i>et al.</i> (2001)
dynamic surface tension measurements: contaminated water	YES	Masutani (1988) Chang and Franses (1994) Huo (1998) Crooks <i>et al.</i> (2001)
bubble dynamics: modeling	YES	Marangoni (1871) Prandtl (1934) Haberman and Morton (1953) Moore (1959) Batchelor (1967) Marucci and Nicodemo (1967) Kunii and Levenspiel (1969) Edwards <i>et al.</i> (1991) De Kee and Chhabra (2002)
bubble dynamics: measurements	YES	Haberman and Morton (1953) Calderbank <i>et al.</i> (1970) Sherwood <i>et al.</i> (1975) Zlokarnik (1980b) Bhaga and Weber (1981) Fan and Tsuchiya (1990) Rodrigue <i>et al.</i> (1996) De Kee and Chhabra (2002) Tzourakos <i>et al.</i> (2004)

3. EXPERIMENTAL DATASETS

The datasets analyzed in this study were compiled by assembling available data from previous investigations in our laboratory (Masutani, 1988; Huo, 1998). These data included both time-dependent and time-integrated measurements. Both Masutani and Huo utilized a maximum bubble pressure method (MBPM) for the time-dependent measurements, thus recording dynamic surface tension (DST). Concurrently, mass transfer coefficients were measured by recording the time variation of dissolved oxygen (DO) concentrations within the testing volume.

A second set of data was collected with an aeration apparatus. These time-integrated datasets include surface tension values as well as mass transfer coefficient values. Surface tension values in these datasets approach those at equilibrium, as they are collected in the DST plateau region (long-time limits). However, these data are not equilibrium surface tension values, which are instead recorded with the du Nuüy ring method.

3.1. Data from Masutani (1988)

These include solutions of sodium tetradecyl sulfate (under the Union Carbide trade name of Tergitol 4, $C_{14}H_{29}NaO_4S$, F.W. 316.43, CAS 1191-50-0) and SDS (sodium n-dodecyl sulfate, $C_{12}H_{25}NaO_4S$, F.W. 288.38, CAS 151-21-3). Both SDS and Tergitol are

commercially available surfactants. SDS, commercially known as sodium lauryl sulfate, is the most common surfactant present in soaps and detergents. Tergitol was chosen because of its higher molecular weight, to investigate differences in surface tension and mass transfer depression related to different molecular weights. Equilibrium surface tension measurements, and concurrent dynamic surface tension and mass transfer measurements were taken.

3.2. Data from Huo (1998)

The chemicals used in these tests were SDS from four different manufacturers and IAA (3-methyl-1-butanol or iso-amyl alcohol, $C_5H_{12}O$, F.W. 88.15, CAS 123-51-3).

SDS was chosen for its frequency of occurrence in wastewater applications, and IAA for its smaller molecular weight, to extend the range of investigations from previous data collected analyzing Tergitol. Consistently with Masutani's datasets, equilibrium surface tension measurements, and concurrent dynamic surface tension and mass transfer measurements were taken.

3.3. Equilibrium surface tension measurements

In both the studies by Masutani and Huo, equilibrium surface tension was measured using both the capillary rise method and the Du Nuöy ring method (Lecomte du Noüy, 1919).

The capillary apparatus utilized is from Fisher Scientific (Cat. No. 14-818), consisting of

a 250 mm borosilicate glass capillary tube, graduated from 0 to 100 mm in 1 mm increments. The capillary radius of 0.35 mm was determined by measuring the surface tension of pure benzene in a thermostat-controlled bath at 20°C and 40°C.

The du Nuöy ring method depends upon the determination of the maximum pulling force necessary to detach a circular standardized ring of round wire from the surface of a liquid with a zero contact angle. Du Nuöy ring method measurements were performed using a Fisher Surface Tensiomat (Model 21), which is essentially a torsion balance. A Pt-Ir ring connected to a torsion arm is used to measure the surface detachment force. The Tensiomat was used in the semi-automatic mode to increase reproducibility. The apparent surface tension measurements collected with the ring method were converted to absolute values with the introduction of correction factors available in literature (Harkins and Jordan, 1930; Freud and Freud, 1930). The deionized water was obtained with a Barnstead NANOpure Infinity ultrapure water system (resistivity, 18 M Ω -cm).

3.4. Dynamic surface tension measurements

Dynamic surface tension measurements were collected to obtain a time-dependent dataset. A maximum bubble pressure method (MBPM) instrument was constructed and is illustrated in figure 3.1.

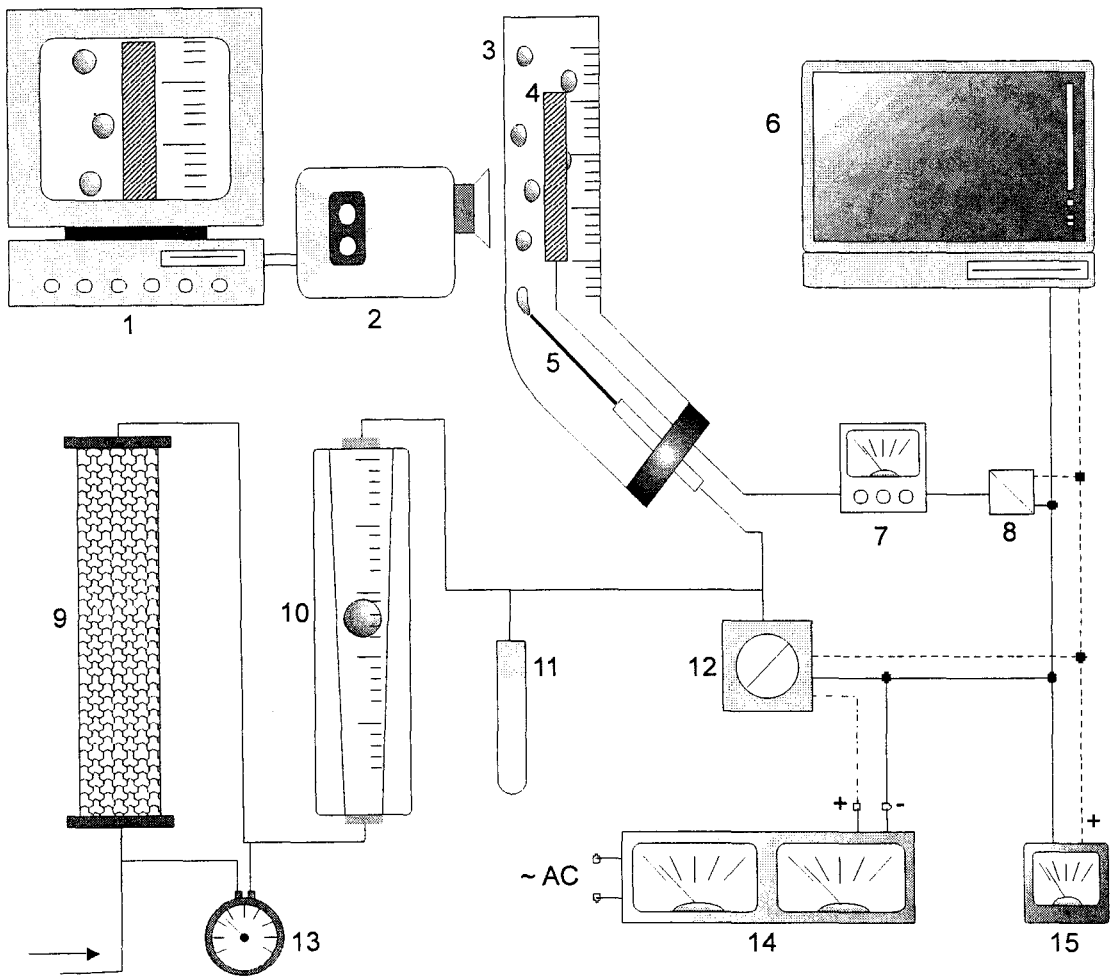


Figure 3.1. Dynamic surface tension measuring apparatus, based on the maximum bubble pressure method (Masutani, 1988; Huo, 1998). Key: computer for image recording (1), camcorder (2), square graduated glass tube (3), micro-O₂ electrode (4), capillary needle (5), computer for signal logging (6), dissolved O₂ meter (7), A/D converter (8), desiccator (9), rotameter (10), buffer vial (11), pressure transducer (12), pressure gauge (13), power supply (14), voltmeter (15).

In this set-up, the air tubing was passed through a desiccator (DRIERITE Gas Purifier, Model L68GP) to remove water vapor, which causes pressure fluctuations. Downstream from an airflow meter (Cole Parmer, 0-7 ml/min scale) the air line was split into three lines. The first line was directed to a pressure transducer (Setra Systems, Model 264 D-10) connected to a power supply. The pressure transducer senses the differential pressure and converts it to a voltage for both unidirectional (0-10 V) and bi-directional (± 5 V) pressure ranges. The second line is connected to a 40ml glass vial serving as a gas buffer chamber. This vial helps maintain constant pressure in the air line through bubble formation and release. The third line is connected to a fused silica needle syringe with a Pyrex round capillary needle (Wilmad Glass, 0.15/0.25 mm internal/outer diameters, 100 mm long) releasing bubbles into a square graduated Pyrex glass tube. Bubble diameters were measured by photographing the rising bubbles with a video camera operating at high shutter speed (10,000 frames/second, f 1:1.8, +18dB gain). The apparatus returns a voltage signal as in figure 3.2.

Mathcad Plus was used to calculate bubble frequencies using a Fast Fourier Transform algorithm and a Visual Basic code was used to collect all data and calculate surface tension from voltage values. The set-up used by Huo varied from the previous set-up by Masutani only in utilizing a newer digital/analog converter.

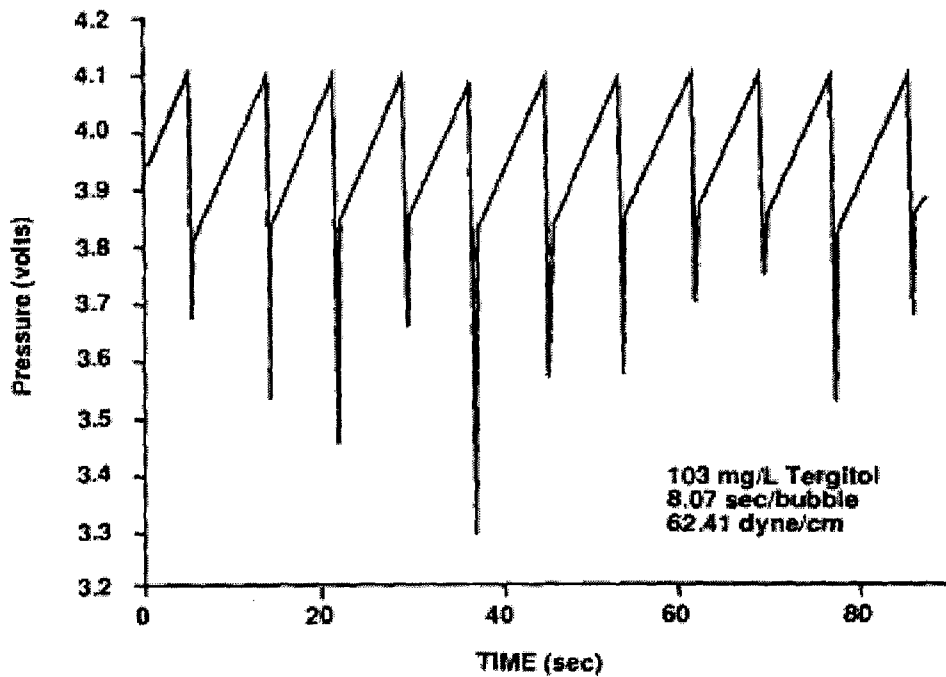


Figure 3.2. Typical bubble formation pattern (Masutani, 1988).

3.5. Mass transfer coefficient measurement

A micro-O₂ electrode (Microelectrodes, Model MI-730) was placed inside the square graduated Pyrex glass tube. This was used to measure concurrently mass transfer coefficients while also measuring DST and bubble diameters. Mass transfer measurements were performed by integrating the differential mass balance for the dissolved O₂ concentration [DO] as in the model of eq.2.1. Oxygen concentrations and voltages were acquired via an analog/digital converting board connected to a computer. This procedure follows a standardized protocol, and is available in literature (ASCE, 1984, 1991; ATV-DVWK 1996; prEN 12255-15, 1999).

Time-integrated measurements were performed on SDS and Tergitol (Masutani, 1988) and on SDS and IAA (Huo, 1998) solutions in a 200 liters diffused aeration vessel (figure 3.3).

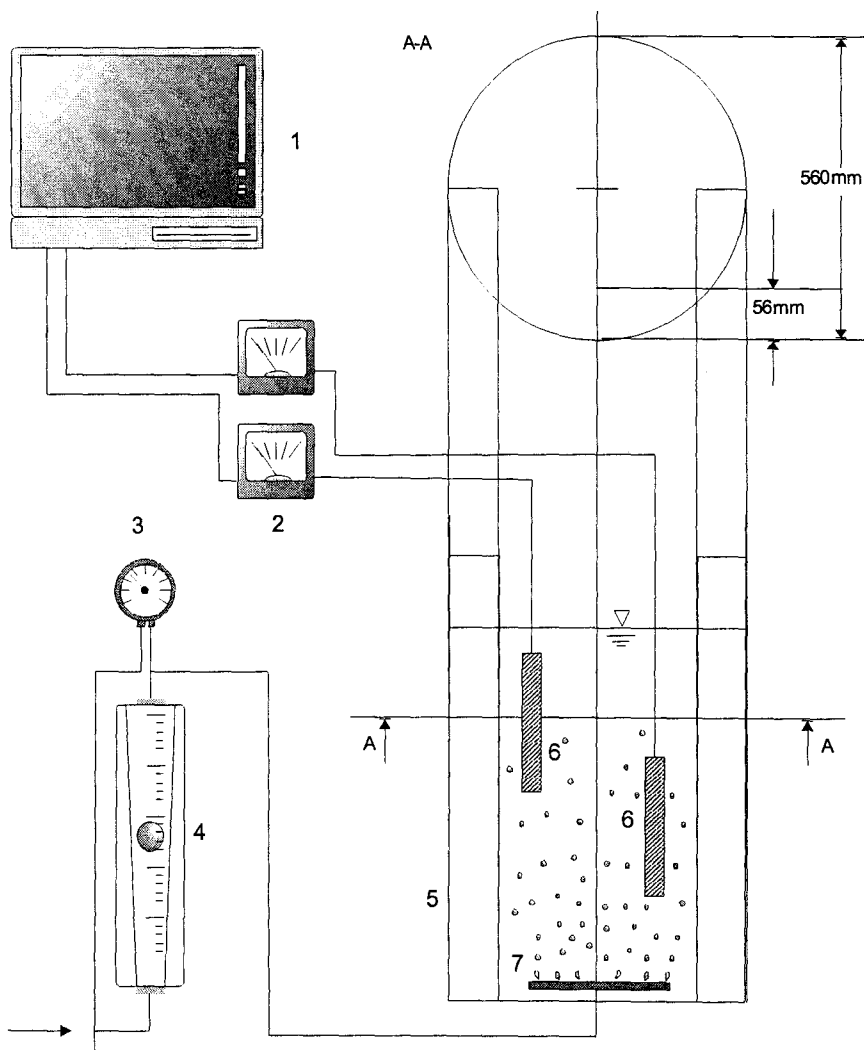


Figure 3.3. Aeration apparatus. Key: computer for signal logging (1), dissolved O₂ meters (2), pressure gauge (3), rotameter (4), aeration vessel (5), dissolved O₂ probes (6), aeration device (7).

Fine bubbles were distributed through the bottom of the aeration vessel with a fine-pore ceramic aerator at airflow rates of 8, 12, and 20 l/min. Two oxygen probes were used, and their values averaged. These data were included in the present study to extend time-dependent data to higher flow rates and longer bubble lives.

The older datasets by Masutani did not contain mass transfer measurements for all experiences. In order to complement the data, penetration theory (Higbie, 1935) was used (eq.2.8).

3.6. Remarks on raw data

SDS Concentrations were normalized to the CMC value available in literature of 2360 mg/l (Rosen, 1978). Thus, by defining the reduced concentration c^+ as the surfactant concentration over the CMC, $\ln(c^+)$ will be equal to 0 at the CMC. In the same way, the measured value of the static surface tension of pure water ($c^+ = 0$) was used to normalize the vertical axis. At zero contamination ($\ln(c^+) \rightarrow -\infty$), the surface tension is same as clean water (Fig. 2.10).

Figure 3.4 shows results from MBPM measurements of SDS solutions taken in a controlled temperature environment ($\pm 0.3^\circ\text{C}$). In this graph the dynamic surface tension $\gamma(t_B)$ is plotted versus time. Solutions with higher SDS concentrations have higher slope due to higher surfactant interfacial accumulation. At very long-time limits, all slopes will reach plateaus. At the initial time range, the surface tension remains at approximately the

value of clean water, and starts to decrease only after a lag time (see also fig.4.1). Higher concentrations will show a shorter lag-time and a lower equilibrium surface tension, due to larger quantities of contaminants accumulating on the bubble surface over time.

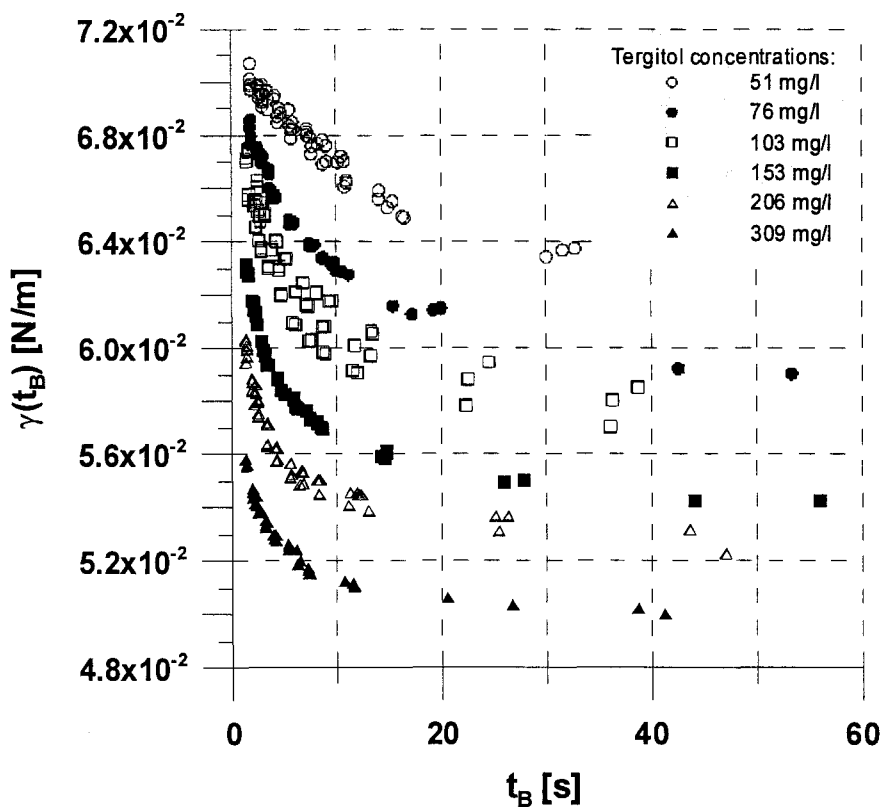


Figure 3.4. Sample DST measurement on Tergitol solutions (Masutani, 1988).

The lag behavior is due to the fact that concentrations in fig. 3.4 are below CMC.

Therefore, there is no excess of surfactant in the solution and the surfactant needs a finite

travel time to contaminate the surface. As the concentration approaches CMC, the lag time reduces in length, and when the concentration is above CMC there exists a surfactant excess in the solution, and the surface contamination effect is immediate, i.e. without lag. Several tests reported in literature show no lag time for surfactant concentrations above CMC (Datwani and Stebe, 2001; Daniel and Berg, 2003). Also, concentrations higher than the CMC will show a dynamic surface tension pattern converging to the same plateau, as the equilibrium surface tension above CMC does not vary (figure 2.10).

Figure 3.5 shows values of the volumetric liquid-side mass transfer coefficient $k_L a$. Several runs were performed for each elapsed time, and bars represent one standard deviation. The volumetric mass transfer coefficient is calculated from dissolved oxygen concentration values using eq.2.1. The dissolved oxygen measurements were taken concurrently while measuring $\gamma(t_B)$.

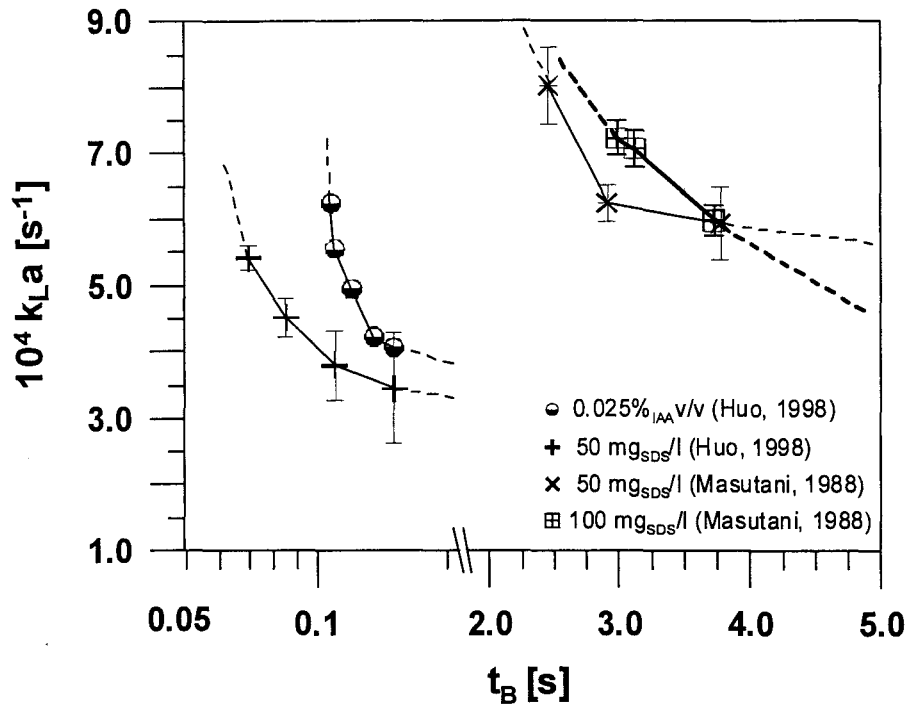


Figure 3.5. Mass transfer coefficient measurements. Bars represent one standard deviation (IAA not visible because the standard deviation is too small).

Comparing figs.3.4 and 3.5 we can observe that both mass transfer coefficients and dynamic surface tension decline rapidly with time, and that they are directly correlated. This was the main conclusion by both Masutani and Huo.

4. RESULTS AND DISCUSSION

4.1. Preliminary results

In this section preliminary results from the previous investigations by Masutani (1988) and Huo (1998) are presented. The datasets contain a much wider amount of data to be plotted, but for the sake of brevity only some selected results representative of the whole are presented. Furthermore, one of the goals of the present work is to unify the available data in a generalized, dimensionless fashion. The results presented and discussed in § 4.3 will serve this purpose. The definition and meaning of all dimensionless numbers used in this chapter are reported in detail in table 4.2.

Figure 4.1 shows the dynamic surface tension $\gamma(t_B)$ and the surface accumulation $\Gamma(t_B)$ for a selected time-dependent measurement (Huo, 1998). For both parameters γ and Γ , the trends in fig.4.1 have analogous explanations. After the initial lag time, migration of contaminants towards the interface begins, and reaches a plateau at long-time limits.

The initial lag time is characteristic of the migration of SAA molecules towards the surface. Increasing SAA concentrations show reduced lag times, i.e. the decline in DST values will begin earlier in time. At CMC or higher SAA concentrations, the lag time will approach zero, as there will always be an excess of SAA molecules (in the form of dispersion or micelle) in the proximity of the gas-liquid interface that will instantaneously accumulate on it at formation.

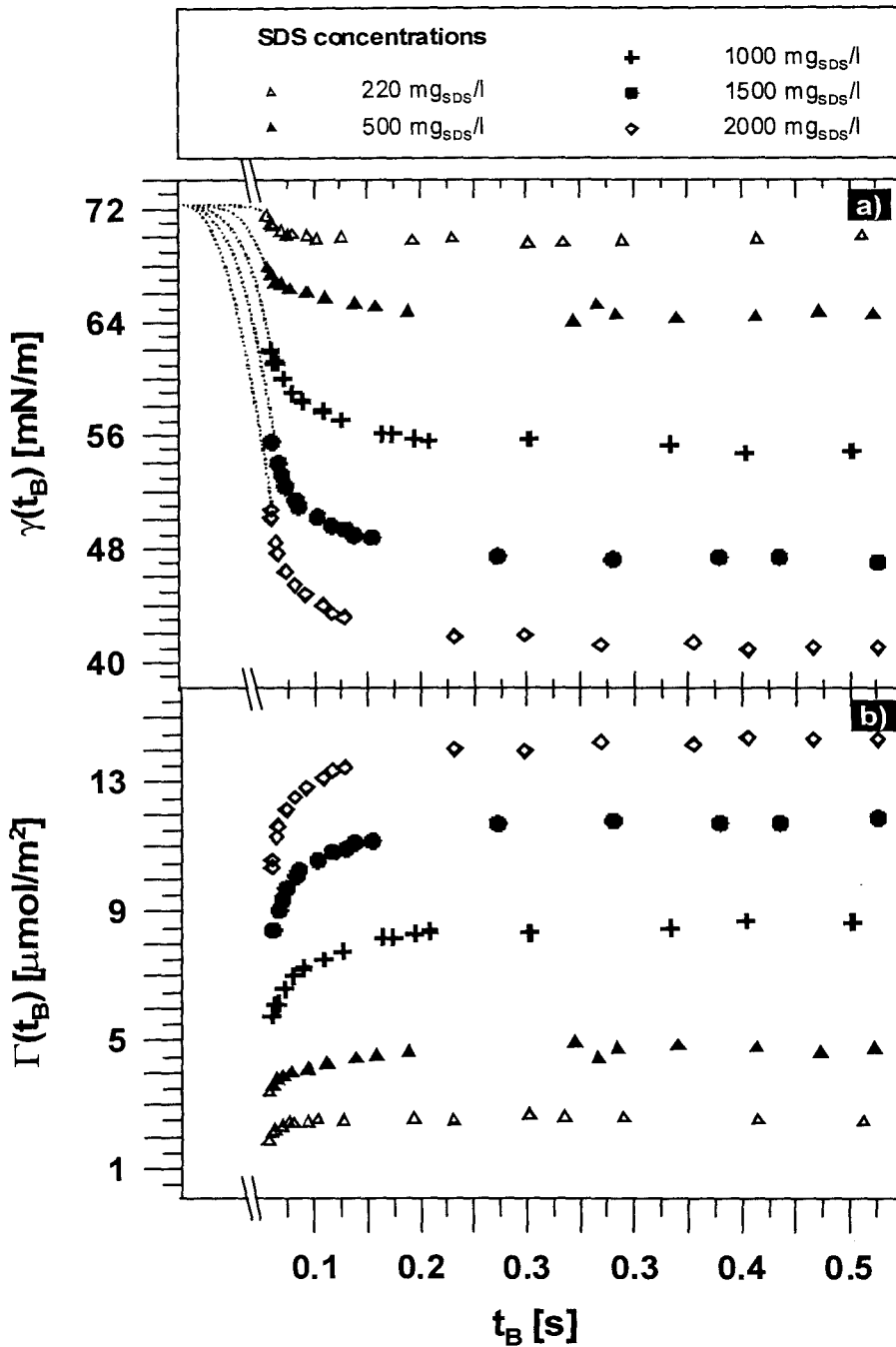


Figure 4.1. a) Dynamic surface tension curves for solutions of sodium dodecyl sulfate (data from Huo, 1988). b) Interfacial excess accumulation calculated with eq.2.19. Dotted lines are expected trends.

The plateau behavior shows the partition equilibrium between the solution and the surface contamination for each given concentration. Higher bulk surfactant concentrations result in lower plateau values, i.e. higher surface accumulations and lower DST values, until CMC is reached. Again, for concentrations above CMC, the dissolved surfactant mass in excess to the CMC will form micelles, thus not contributing to the surface accumulation. This is observed in higher contamination limit plateaus and lower DST limit plateaus.

The surface accumulation was calculated with both eqs.2.19 and 2.23, i.e. by using both the Langmuir and the Ward-Tordai adsorption models, respectively. Fig. 4.2 shows a comparison of the two results. The Ward-Tordai method gives a time-dependent solution derived from diffusivity, time, and geometrical parameters, while the Langmuir approach derives phenomenologically the surface accumulation directly from its effect, i.e. the dynamic surface tension change. At short-time limits, the Langmuir equation overestimates the results of the Ward-Tordai equation, yet within the same order of magnitude. At long-time limits, the two equations tend to same results, and their ratio approaches unity (see fig.4.2).

As time increases, the effect of liquid-side surfactant accumulation is reflected in the gas-side. Figure 4.3 shows the concurrent interfacial phenomena occurring from the liquid- and gas-side during the formation and detachment of a series of single bubbles in 50 mg/l of Tergitol. The top-half of figure 4.3 shows a normalized plot of the evolution of liquid-side surfactant interfacial diffusivity with increasing time. This parameter was calculated

with the Hansen limit of the Ward-Tordai model (eq.2.24) and divided by the surfactant bulk concentration.

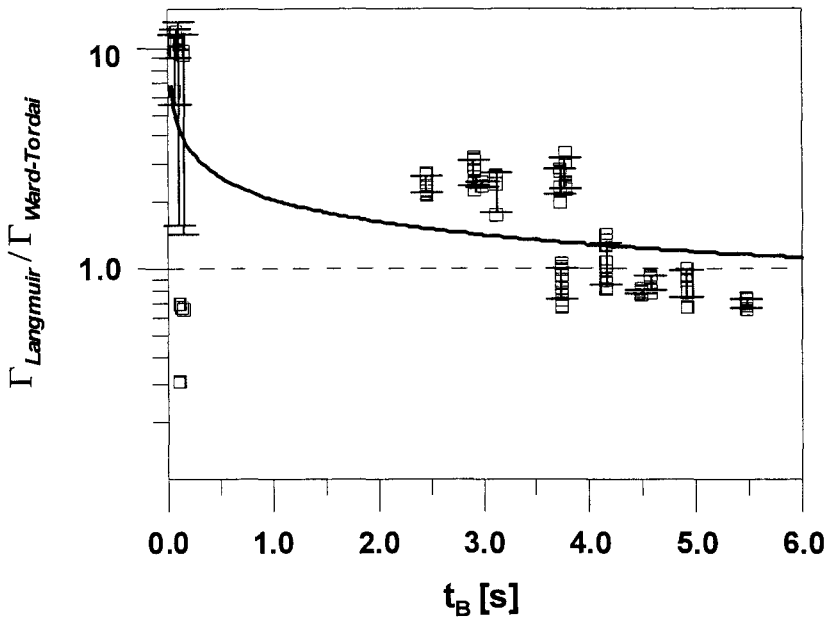


Figure 4.2. Surface accumulation calculated with the Langmuir and Ward-Tordai adsorption models. Bars represent one standard deviation and the trendline is a logarithmic best-fit.

At the beginning of bubble formation, the interfacial surfactant diffusivity shows a discontinuity and peaks to a value about one order of magnitude higher than its bulk concentration, driven by Van der Waals exclusion forces. As the bubble formation progresses, the surface saturation [plotted in the same graph as $\Gamma(t_B)/\Gamma_{eq}$] increases and tends to its maximum value at infinite time, never reached within the length of this experiment's bubble age. At infinite time-limits, the normalized surfactant diffusivity

would reach unity, as the diffusivity would equal bulk values when the surface is saturated at equilibrium with the bulk solution. Thus, the surfactant interfacial diffusivity represents the driving force of the interfacial migration process, as it instantaneously peaks at bubble detachment and declines towards a constant value at equilibrium.

In the bottom-half of fig.4.3 gas-side interfacial diffusivity, calculated by solving Higbie's formula (eq.2.10), is plotted in analogous, normalized fashion. Again, at bubble detachment the newly formed interface experiences practically no contamination for the first instant, when the interfacial diffusivity tends to bulk values. As time progresses, the normalized oxygen diffusivity rapidly declines with time about an order of magnitude below the bulk diffusivity value ($\sim 10^{-10} \text{ m}^2/\text{s}$) and reaches a steady, reduced value when approaching a plateau towards equilibrium.

Figure 4.4 shows results from concurrent DST and mass-transfer measurements, and reports mass transfer time-series as in fig.3.5. It is evident from the graph that mass transfer and dynamic surface tension are directly correlated. This is due to the surfactant that, by accumulating on the interface, lowers the surface tension and reduces interfacial renewal, thus causing lower mass transfer. In figure 4.4 trendlines are linear regression best fits, and two of them are dashed to highlight that same concentrations of the same surfactant ($50 \text{ mg}_{\text{SDS}}/\text{l}$) result in same DST vs. $k_L a$ behavior.

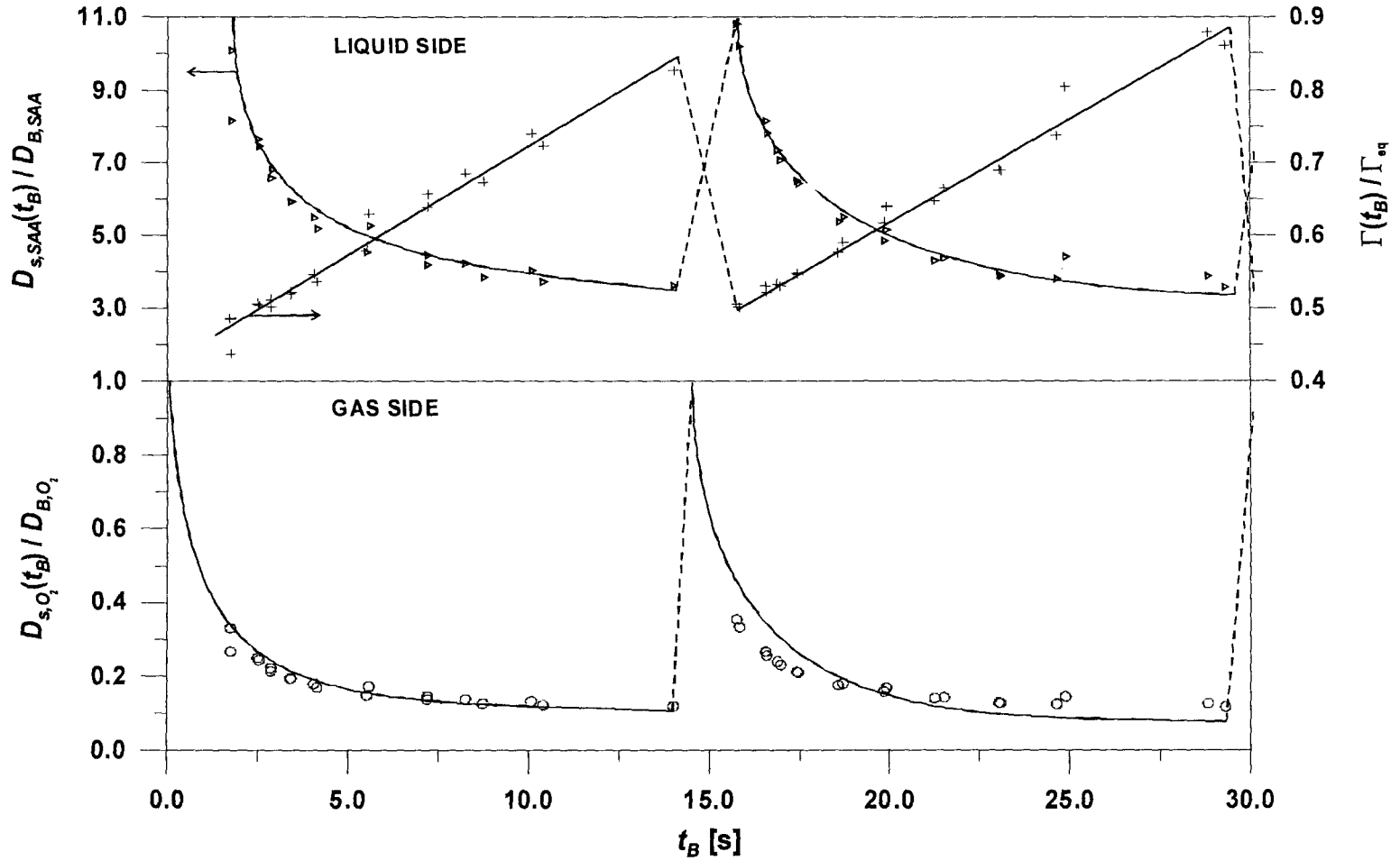


Figure 4.3. Concurrent interfacial phenomena for a single bubble. Diffusivities on the left vertical axis are reduced (interface/bulk). $\Gamma(t_B)/\Gamma_{eq}$ is the normalized surface accumulation. Dashed lines represent expected paths between bubbles.

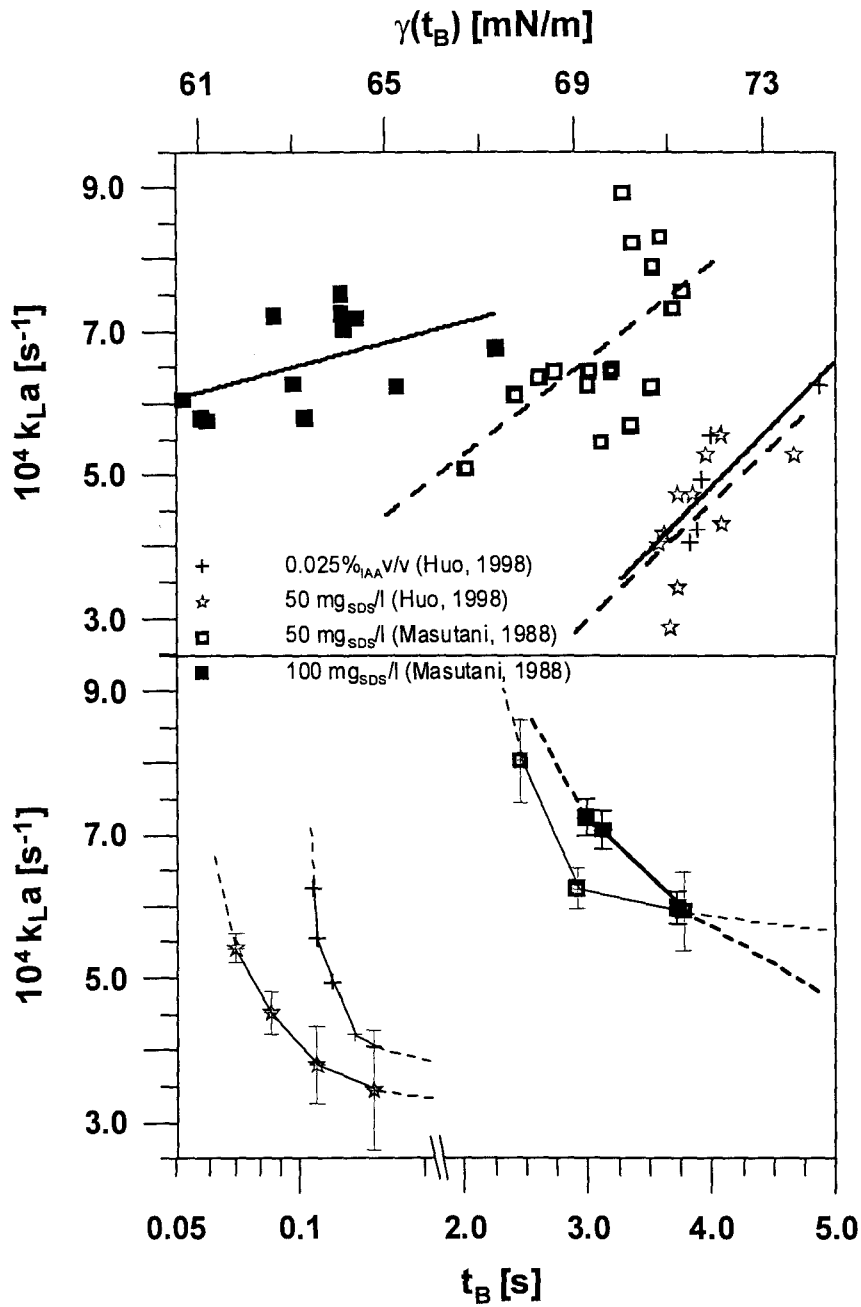


Figure 4.4. Concurrent DST and mass transfer measurements (data from Masutani, 1988; Huo, 1998). Bars on bottom graph represent one standard deviation, with selected points plotted only at averages. Bars for IAA are too small to show on graph.

In figure 4.4, mass transfer coefficient measurements by Masutani have in general higher values than the coefficients measured by Huo. This occurs because the flow regime in Huo's experiments was significantly lower than the flow regime previously adopted. However, different flow regimes have different mass transfer coefficients, and it is necessary to limit the comparison between contaminant concentrations within the same flow regime. Nonetheless, data patterns for 50 mg_{SDS}/l appear similar but shifted on the graph.

The first conclusion can be drawn with this figure, and successive data analyses will corroborate it: higher flow regimes result in higher interfacial renewal rates, hence in a retardation of the surface contamination effects. Moreover, the equilibrium value of the mass transfer coefficient will be higher for higher flow regimes, as the mass transfer is also proportional to the interfacial velocity (plateaus at long-time limits in the bottom-half of the graph).

IAA causes a more rapid decline in mass transfer, which can be identified by the more rapid decrease in $k_L a$ vs. time in the bottom-half of fig.4.4. This is due to its lower molecular weight and its higher velocity of migration towards the interface. In fact, IAA diffusivity ($\sim 10^{-9}$ m²/s @ 25°C) is higher than SDS diffusivity ($\sim 10^{-10}$ m²/s @ 25°C). In general, because of this property, surfactants with higher migration velocity are usually referred to as fast surfactants (Ferri and Stebe, 2000). Conversely, surfactants with lower migration velocity are usually named slow surfactants. IAA also acts on mass transfer

after a longer lag time, but this results because of its different chemical nature and higher flow regime.

4.2. Discussion

In the data by Masutani the patterns for 50 and 100 mg/l SDS intersect at longer-time limits (at $t_B \sim 4s$). After this intersection the mass transfer behavior for the higher SDS concentration reach a lower equilibrium value, since both experiments (at 50 and 100 mg_{SDS}/l) were conducted at the same flow regime, hence at the same surface renewal rate, and higher mass transfer depression occurs at higher contaminant concentration. Still, interfaces with higher renewal rates have a smaller variation due to different contamination than interfaces with same contamination and different flow regimes. By comparing the magnitude of contamination and flow regime effects, we can conclude that higher flow regimes can offset the effects of contamination.

Surface tension values decrease rapidly starting with low contamination. In the case of pure water, H₂O molecules are organized at the interface in a lattice which is in a dynamic equilibrium state (i.e., the interfacial layer is continuously renewed, and each molecule is mainly subject to the hydrogen bond interaction of its neighboring fellow molecules). At zero contamination, the distribution of tensile stresses on the interface is uniform and their statistical sum is null, hence the spherical shape of the bubble. When contaminants are present, the lattice made of water molecules is divided in sub-lattices

that are separated by surfactant molecules. The energy required for the division of the water surface into sub-lattices is provided by the Van der Waals exclusion forces. Due to the nature of surface active agents, hydrogen bonds between surfactants and sub-lattices will not establish, and each sub-lattice will not experience the hydrogen interaction of neighboring ones because of their distance forced by surfactant molecules (SAA molecules have in general molecular radii several fold the molecular radius of water molecules). The overall effect is a lower force required to separate sub-lattices from each other (i.e. lower surface tension). A higher number of accumulated surfactant molecules will result in smaller sub-lattices, therefore lower surface tension for higher contaminations.

The intuitive concept of “molecular obstruction” is usually considered the cause of mass transfer depression. This phenomenon is dominant for stagnant gas-liquid interfaces, where the interfacial fluid velocity is zero. In this case, molecular diffusion through the stagnant film is the only transport mechanism. In case of moving interfaces, turbulent transport towards the interface is the driving force for mass transfer, for two reasons: interfacial renewal rates and actual area covered by the surfactant molecules.

In the case of moving interfaces, which is the case for environmental aeration applications such as diffused and surface aerators, turbulence exists behind the interfacial laminar films. At a given interfacial flow regime, hence at a given interfacial (Re), the film renewal rate is decreased with increasing contamination. This is observed in lower internal gas circulation rates in bubbles (Garner and Hammerton, 1954; Griffith, 1960).

Roy and Duke (2004) photographed two-dimensional dissolved oxygen concentration gradients near surfaces contaminated with the surfactant Triton X-100, using a laser-induced fluorescence technique. Their photographs show reduced circulation outside contaminated bubbles, with higher interfacial O_2 concentration gradients for higher contaminations.

Surface tension is inversely proportional to the boundary layer thickness (Azbel, 1981). Thus, higher contaminations result in higher boundary layer thickness, associated with lower surface tension values. Higher boundary layer thicknesses create a lower probability for a turbulent eddy to reach the interface and carry a “fresh” gas packet from the bulk, i.e. resulting in lower renewal rates (remember the Higbie or Danckwerts models for gas transfer into agitated liquids, §2.1.3). Fig.4.5 shows a re-plot of the data in fig.4.4 including quantitative information on the flow regime, expressed as interfacial (Pe) numbers. The higher mass transfer coefficients resulting from higher interfacial velocities (characterized by higher Péclet numbers) are visible in the plot. Same contaminations can yield different mass transfer coefficients in different flow regimes; therefore, we must conclude that the molecular obstruction phenomenon has a negligible effect on this mass transfer process.

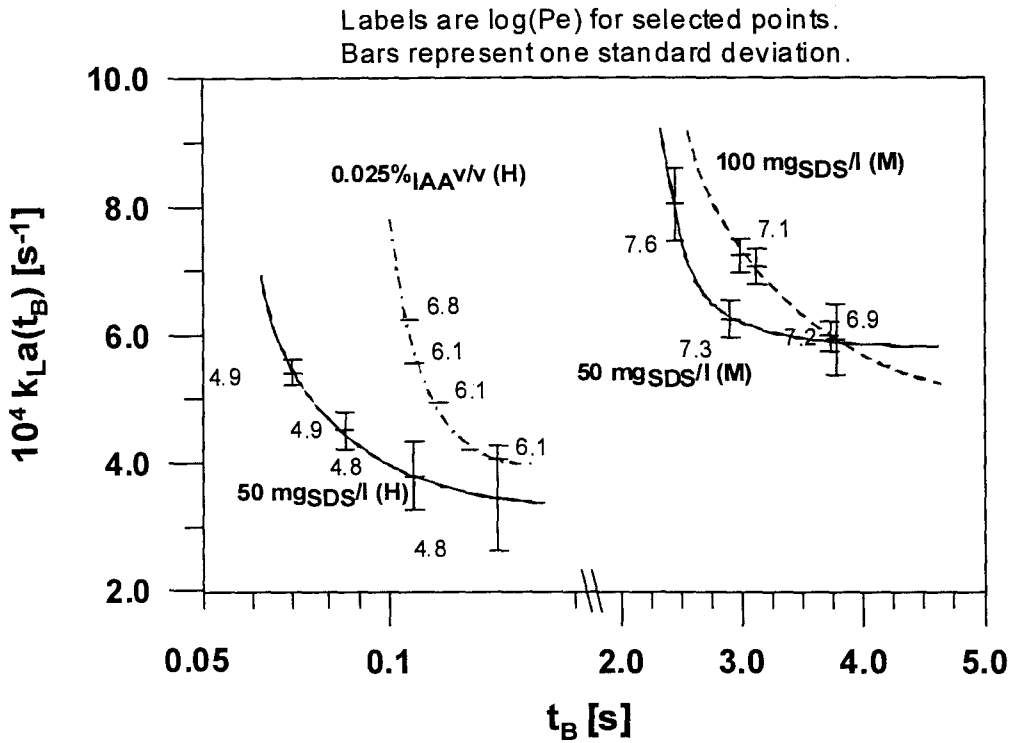


Figure 4.5. Flow regime effects on mass transfer time-series.

Another consideration about the molecular obstruction theory is the effective diffusional area available for O_2 molecules to travel across the interface. Oxygen is present within the bubble at 20.95% v/v concentrations, while the surfactant accumulates on the bubble surface in much lower quantities. Furthermore, due to the nature of the surfactant, its polar head is anchored to the interface, and the hydrophobic tail is fluttering into the bubble volume (fig.4.6). Due to same charge repulsion, surfactant heads will not experience direct contact with each other, leaving always open space amongst them, even

in the most limit case of full surface coverage. Also, the molecular diameter for an oxygen molecule does not exceed 0.3nm, while the diameter of the surfactant head is on the order of 10nm or more. The frontal diameter to account for the surfactant is the diameter of the polar head, as the hydrophobic tails are inside the bubble, where gas molecules are free to move by virtue of molecular diffusion.

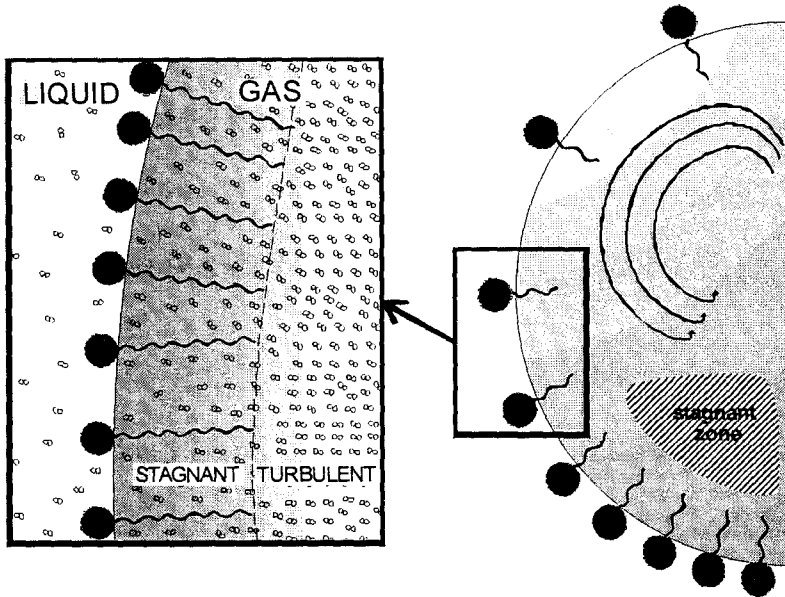


Figure 4.6. Schematics of surfactant interfacial accumulation and its reduction of gas turbulence.

If the molecular obstruction phenomena were dominant, reduced transfer should also occur for salts and certain aliphatic alcohols, which show mass transfer enhancement (i.e., $k_L a_{pw} > k_L a_{cw}$, or $\alpha > 1$), instead of depression (Zlokarnik, 1980a). For the range of surfactant accumulation of the present datasets, the number of O_2 molecules far exceeds

the number of surfactant molecules. The interfacial accumulation of surfactant molecules is different at different angles from the front stagnation point (i.e., the highest point of the rising bubble), and the ratio between fore- and aft- accumulation was recorded to vary between 10 to 100 times at $(Pe) = 10^5$ (Ramirez and Davis, 1999). The interfacial ratio of surfactant to oxygen molecules for the tests analyzed in this study was calculated and exceeded 1/100 on an average around the bubble and 1/1000 on the upper cap of the bubble. If molecular obstruction is assumed as dominant, it should be the same for both high and low interfacial velocities. Nevertheless, mass transfer depression has a higher magnitude at lower interfacial velocities, confirming that molecular obstruction is negligible for flowing systems.

Fig.4.7 shows a photograph at 1/500" of coarse- and fine-bubbles in a 50mg_{SDS}/l solution, and the schematics of inner fluid dynamic patterns. It is visible that the large majority of fine-bubbles have a diameter lower than 1mm. Clean water tests without surfactant in analogous conditions yielded bubble mean diameters of 4 mm, larger than any bubble in contaminated water. In fig.4.7, one fine- and one coarse-bubble are highlighted and their interior circulation patterns are sketched to the side. The accumulation of surfactant at the fine-bubble interface occurs in larger extent than for coarse-bubbles, as the hydraulic residence time is higher, and surfactant molecules have longer time available for migration towards the interface.

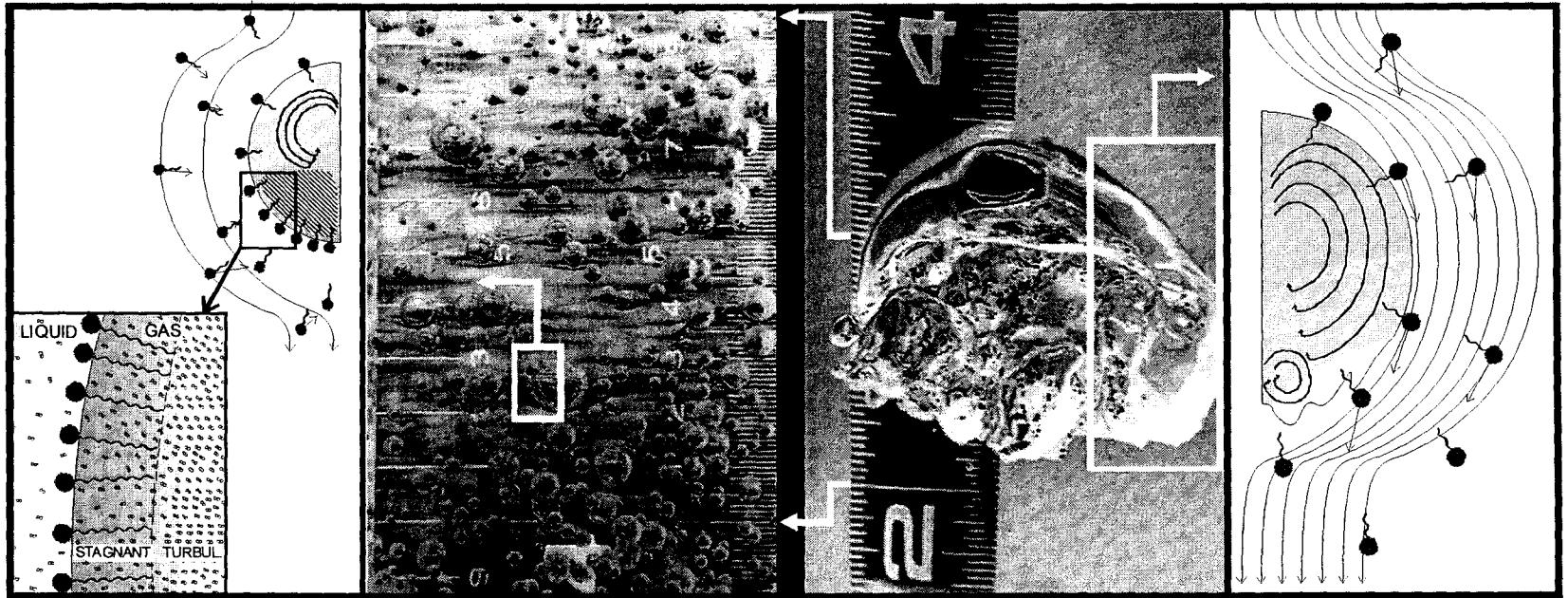


Figure 4.7. Comparison of fine- (left photograph) and coarse- (right photograph) bubbles generated by two different aerators operating at same airflow rate in the same surfactant solution (50 mg_{SDS}/l). The scale in the photographs is in inches. The fine-pore aerator is a 150x150mm (6x6in) panel mounting a Vyon P Porvair plastic sintered membrane with mean porosity of 9 μ m. The coarse bubble aerator is a 9.53 mm (3/8 in) air nozzle. The outer drawings show the different mechanism of interfacial accumulation in the two cases. The scale in this figure is in inches (25.4 mm), with subdivisions in 0.1 in (2.54 mm).

Furthermore, smaller bubbles have much lower interfacial velocity, and once the surfactants have attached to the surface, their hydrophobic tails inside the bubble reduce the internal gas circulation, acting like a baffle in a stirred reactor. Surface active agents tend to accumulate at the bottom of the bubble, creating a stagnation zone inside the bubble, usually referred to as stagnant cap. Evidence supports the existence of fore-and-aft symmetry in the concentration distribution at the interface (Clift et al., 1978; Ramirez and Davis, 1999).

Additional photographs were taken at 1/125" and used to calculate the bubble mean rising velocity, which is approximately 0.2 m/s for fine-bubbles and 1.5 m/s for coarse-bubbles in fig.4.7. With large interfacial area and large mass transfer time, fine-bubbles should have a very high $k_L a$. Yet, mass transfer coefficients in surfactant solutions are smaller than mass transfer coefficients in clean water, even though the bubble diameters are larger in clean water (i.e., smaller specific interfacial area). Therefore, the mass transfer times in clean water are reduced due to greater rise velocities. For coarse-bubbles the differences between clean- and process- water transfer rates are reduced, due to higher interfacial velocity and higher rate of turbulence.

4.3. Dimensionless presentation of results

In order to generalize the results and compare different flow regimes, geometries and contaminations, a dimensional analysis was performed. When dimensional analyses are

performed on experimental data, the correlations are reported in dimensionless form, thus normalizing results for physicochemical and process-specific variables. The results presented in this fashion will then show one trendline *in lieu* of a family of parametric curves. The method used is based on the Buckingham pi theorem, and the procedure is by Zlokarnik (2002). The physical quantities included in the analysis were: bubble life t_B , mass transfer coefficient $k_L a(t_B)$, bubble diameter $d_B(t_B)$, orifice diameter d_o , dynamic surface tension $\gamma(t_B)$, weight (i.e., buoyancy) of the bubble $g\Delta\rho$, bulk surfactant concentration c_B , oxygen interfacial diffusivity $\mathcal{D}_{s,O_2}(t_B)$, surfactant bulk diffusivity $\mathcal{D}_{B,SAA}$, and airflow rate Q . Due to the low shear rate of this process, the liquid viscosity has no influence and is thereby excluded from the analysis. Highly viscous systems need a different dimensional analysis, because the transport phenomena occurring in those systems are due to different transport mechanisms. The oxygen diffusivity at the surface is the sole time-dependent diffusivity used in this analysis, because the analysis is conducted by observing the whole physical system from the inside of the bubble, i.e. it will result in a gas-side empirical correlation. The surfactant bulk diffusivity will be used in the analysis and the effects on the interface will be reflected to the gas-side by including the time-dependent dynamic surface tension. The use of a time-dependent diffusivity in the analysis will result in redundancy and in problems with statistical significance, as the time-dependent interfacial surfactant diffusivity is calculated via a Ward-Tordai model, function of the dynamic surface tension itself. The liquid-side interfacial diffusivity was indeed calculated with the Ward-Tordai model to corroborate the results of the dimensional analysis, confirming the expectations that gas and liquid

side diffusivities concurrently change with increasing time (Masutani and Stenstrom, 1991; Ferri and Stebe, 2000).

A dimensional matrix that includes all nine relevant parameters is compiled (table 4.1). Each value of the matrix represents the exponent of the physical quantity contained in each physical parameter. For example, the diffusivity has units of $\text{mass}^0 \cdot \text{length}^2 \cdot \text{time}^{-1}$, hence the numbers for mass, length, and time will be 0, 2, and -1, respectively. By taking linear transformations of the dimensional matrix (the upper matrix above) we can obtain a unity core matrix of the pi-set (zero-free main diagonal, zeroes otherwise; the lower non-shaded matrix in table 4.1).

Table 4.1. Dimensional matrix.

	$g\Delta\rho$	d_B	\mathcal{D}_{s,O_2}	$k_L a$	γ	d_o	c_B	t_B	$\mathcal{D}_{B,SA}$	Q
Mass	1	0	0	0	1	0	1	0	0	0
Length	-2	1	2	0	0	1	-3	0	2	3
Time	-2	0	-1	-1	-2	0	0	1	-1	-1
Mass	1	0	0	0	1	0	1	0	0	0
Length	0	1	0	-2	2	1	3	2	0	1
Time	0	0	1	1	0	0	-2	-1	1	1

From this matrix we generate seven independent dimensional numbers Π_i (table 4.2).

This is done by taking each element of the residual matrix (shaded in table 4.1) as a numerator, and all elements of the unity core matrix in the denominator, each elevated to

the exponent indicated in the residual matrix. The application of this method allows to fully describe the system in its geometrical, chemical, physical, and process-related characteristics.

Table 4.2. Dimensionless numbers, notation and physical significance.

Symbol	Pi-notation	Extended notation	Physical significance
(Sh)	Π_1	$\frac{k_L a \cdot d_B^2}{D_{s,O_2}}$	$\frac{\text{mass diffusivity}}{\text{molecular diffusivity}}$
(Bd)	$(\Pi_2)^{-1}$	$\frac{g \Delta \rho \cdot d_B^2}{\gamma}$	$\frac{\text{gravity force}}{\text{surface tension}}$
d^+	Π_3	$\frac{d_o}{d_B}$	dimensionless length-scale
(Sm)	Π_4	$\frac{c_B \cdot D_{s,O_2}^2}{g \Delta \rho \cdot d_B^3}$	$\frac{\text{surface contamination}}{\text{gravity force}}$
t^+	Π_5	$\frac{t_B \cdot D_{s,O_2}}{d_B^2}$	$\frac{\text{geometrical time scale}}{\text{diffusional time scale}}$
D^+	Π_6	$\frac{D_{B,SAA}}{D_{s,O_2}}$	dimensionless diffusivity
(Pe)	Π_7	$\frac{Q}{d_B \cdot D_{s,O_2}}, \frac{u \cdot d_B}{D_{s,O_2}}$	$\frac{\text{advective forces}}{\text{diffusive forces}}$
(Ro) _I	$\Pi_2 \cdot \Pi_4 \cdot \Pi_6^2$	$\frac{c_B \cdot D_{B,SAA}^2}{\gamma \cdot d_B}$	$\frac{\text{surface contamination}}{\text{surface tension}} \Big _{eq.}$
(Ro) _{II}	$\Pi_2 \cdot \Pi_4 \cdot \Pi_6^2 \cdot \Pi_5$	$\frac{c_B \cdot t_B \cdot D_{B,SAA}^3}{\gamma \cdot d_B^3}$	$\frac{\text{surface contamination (time)}}{\text{surface tension (time)}}$

Π_1 , $(\Pi_2)^{-1}$, and Π_7 are the interfacial Sherwood (Sh), Bond (Bd), and Péclet (Pe) numbers, respectively. Π_3 and Π_5 are named the dimensionless characteristic length d^+ and time t^+ , for sake of clarity. Π_6 is the dimensionless diffusivity, and Π_4 is named the gravitational contamination number (Sm).

Goal of this analysis is to describe the physical system with an empirical correlation between the dimensionless numbers generated. As a starting point of reference, Frössling (1938) performed a dimensional analysis on bubble gas transfer systems that lead to the well-known empirical formula:

$$(\text{Sh}) = a \cdot (\text{Re})^b \cdot (\text{Sc})^c \quad (4.1)$$

where (Sh), (Re), and (Sc) are the Sherwood, Reynolds, and Schmidt (=viscosity/diffusivity) numbers, respectively; a, b, and c are empirical fitting parameters. By its definition, the Péclet number equals Reynolds times Schmidt, or:

$$(\text{Pe}) = (\text{Re}) \cdot (\text{Sc}) \quad (4.2)$$

The bubble-droplet duality allows the use of eq.4.1 for droplets. The Frössling empirical equation relates the gas transfer to the flow regime, with higher mass transfers for higher bubble velocities. At no flow, eq.4.1 predicts zero mass transfer. There are numerous observations in literature for the fitting parameters a, b, and c (Levich, 1962; Acrivos and Goddard, 1965; Lamont and Scott, 1970). Depending on the process conditions, there exist correlations between the model limits of rigid and circulating spheres (Clift et al., 1978). Substituting eq.4.2 in eq.4.1 we obtain:

$$(\text{Sh}) = a' \cdot (\text{Pe})^{b'} \quad (4.3)$$

where a' and b' are empirical constants. The exponent b' is reported to range between the values of $1/3$ for solid surfaces to $1/2$ for circulating surfaces (Levich, 1962; Acrivos and Goddard, 1965; Lamont and Scott, 1970; Clift et al., 1978). Eq.4.3 shows the analogy between mass diffusivity (i.e., the mass transfer coefficient $k_L a$) and advective forces (the bubble velocity u_B).

By defining the surface contamination numbers, for the cases of time-averaged and time-dependent tests:

$$(\text{Ro})_{\text{I,II}} = \begin{cases} (\text{Ro})_{\text{I}} = \frac{(\text{Sm})}{(\text{Bd})} \cdot (D^+)^2 & \text{for time - averaged tests} \\ (\text{Ro})_{\text{II}} = \frac{(\text{Sm})}{(\text{Bd})} \cdot (D^+)^2 \cdot t^+ & \text{for time - dependent tests} \end{cases} \quad (4.4)$$

the physical system can be defined by the pi-set:

$$(\text{Sh}) = f \{ (\text{Pe}), (\text{Ro})_{\text{I,II}} \} \quad (4.5)$$

The dimensionless length-scale d^+ was contained within a narrow range throughout our dataset, and showed no improvement of the regression analysis, and therefore not included. For time-integrated measurements, such as calculations of average mass transfer coefficients for the entire re-aeration process, t^+ has an average value, and carries no time-dependent information; hence the problem can be described by the use of either contamination number. For sake of simplicity, $(\text{Ro})_{\text{II}}$ is used for the final version of the

empirical correlation. Nonlinear regression analysis were performed using SYSTAT 10 (SPSS Corporation, Chicago, IL), showing that the combination of dimensionless numbers

$$(\text{Sh}) = \frac{0.382 \cdot (\text{Pe})^{1/3}}{1 + \log[1 + 10^{19} \cdot (\text{Ro})_{\text{II}}]} \quad (4.6)$$

is statistically significant ($R^2 > 0.8$; $t > 10$; $P < 10^{-3}$; unbiased residuals). The bubbles of this study show to behave like solid spheres, as the exponent of (Pe) approaches 1/3. During preliminary analyses, the exponent of (Pe) departed from 1/3 of less than 10%, and was later fixed to 1/3, thus adsorbing the difference in the updated slope (0.382). Eq.4.6 shows the analogy between mass diffusivity (Sh), advective forces (Pe), and contamination effects (Ro)_{II}. The statistical significance of eq.4.6 was verified with a linear regression analysis of measured vs. estimated log(Sh) values. Details on this verification are reported in table 4.3, and residuals are graphed in fig. 4.8.

Table 4.3. Results of the statistical analysis: estimated vs. calculated (Sh).

General regression				Analysis of variance	
Dep. Var.	log(Sh) _{EST.}	P(2 Tail)	0.000	Standard error of estimate	31.843
Coefficient	0.590	Multiple R	0.814	Sum-of-Squares	197602.53
Std. Err.	0.045	Squared multiple R	0.663	F-ratio	169.2517
Std. Coef.	0.814	Adj. multiple R	0.663	Durbin-Watson D Statistic	0.160
t	13.010			First Order Autocorrelation	0.903

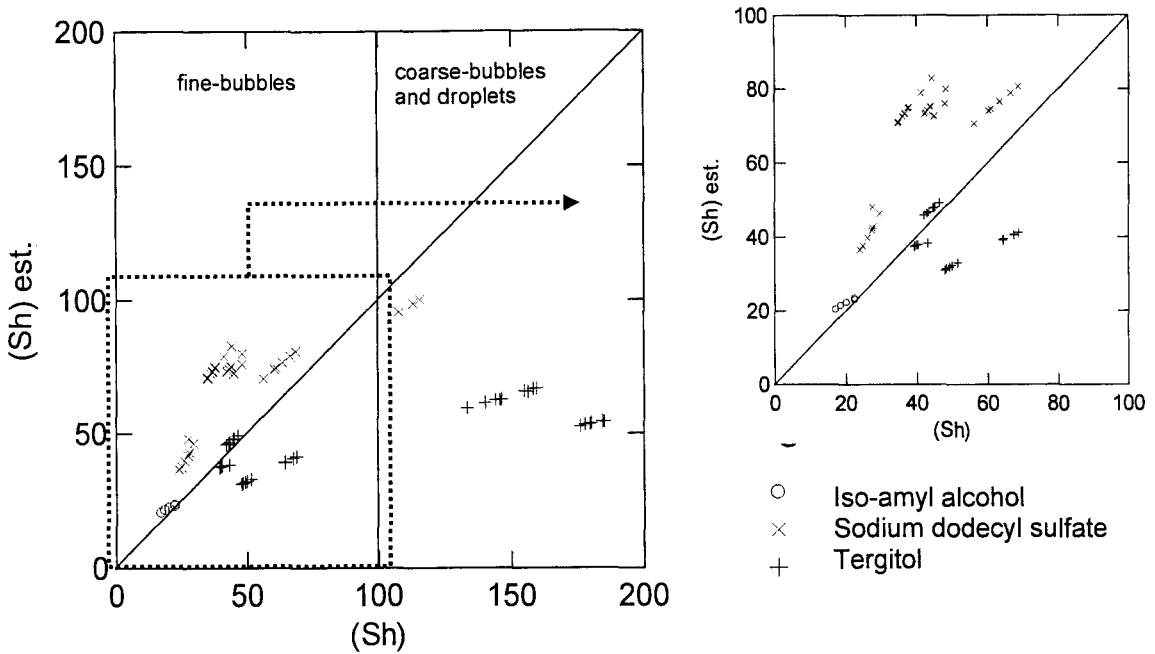


Figure 4.8. Results of the statistical analysis: plot of (Sh) versus estimated (Sh) . Note that for $(Sh) > 70$ eq.4 .6 starts underestimating.

Figure 4.6 shows the plot of (Sh) vs. estimated (Sh) . It is evident that for $(Sh) > 10^2$ eq.4.6 starts departing and underestimating (Sh) values. This is because at in this range the advective forces start having a higher weight than the contamination forces. In this region, the interfacial Péclet number is higher than 10^7 , corresponding to the upper limit of the operating fine-bubble regime. The region $(Sh) < 10^2$ corresponds to interfacial velocities encountered in practical applications of fine-bubbles, whereas to obtain $(Sh) > 10^2$ the energy required per unit volume of liquid would be too high to result in an economically viable process.

In order to present the evolution of mass transfer with increasing time in a dimensionless form, (Sh) was plotted versus the dimensionless time (fig. 4.9). In this log-log plot, the labels represent $\log(Pe)$ for selected points. Note that (Pe) is the interfacial Péclet number, calculated using the interfacial O_2 diffusivity (which is reduced when compared to O_2 bulk diffusivity). As a consequence, (Pe) values in this paper appear higher than (Pe) calculated using bulk diffusivity. Nevertheless, the relative ratio between (Pe) characterizing experiments with different flow regimes and surfactants will remain unchanged. Besides the expected conclusion that (Sh) declines with increasing time, three main results are evident: 1) (Pe) declines over time, 2) the slope of the trends are dictated by the contamination (type of contaminant and concentration), and 3) intercepts, at a given contamination, are dictated by the flow regime, with higher intercepts at higher flow regimes.

The decline of (Pe) is due to the decrease in bubble terminal velocity, due to the concurrent effect of higher drag (due to the contamination) and of bubble reducing in size (due to gas transfer). The oxygen interfacial diffusivity decreases rapidly at the initial phase of contamination, but this effect does not increase (Pe) (the diffusivity is at the denominator, as in table 4.2), because both velocity and bubble diameter appear in the numerator, which declines over time. The overall effect is a slight decline of (Pe) , observable as a slightly lower bubble terminal rise velocity, for all the cases here presented.

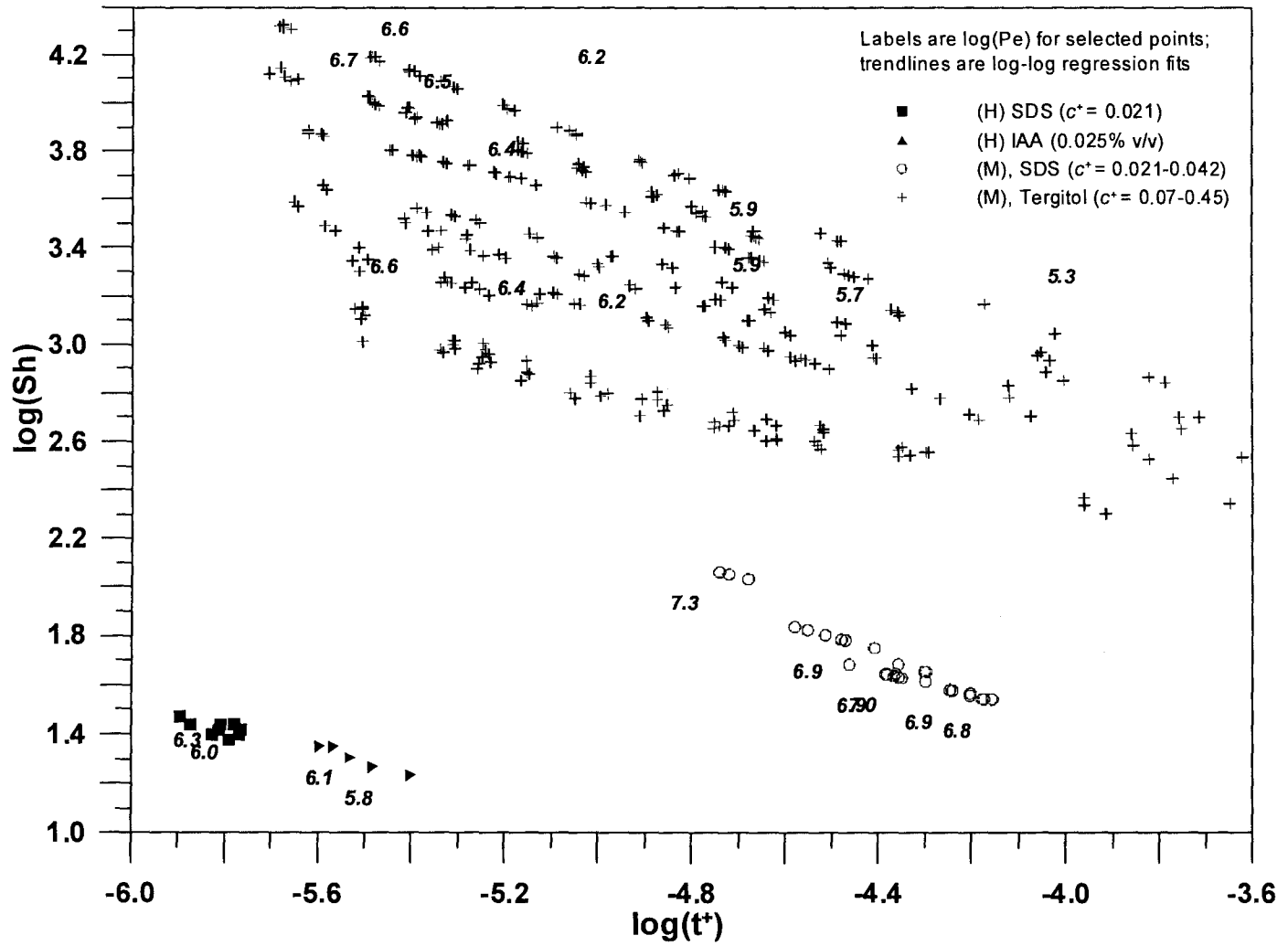


Figure 4.9. Dimensionless representation of mass transfer phenomena with time.

SDS data by Huo (1998) have the same slope as SDS data by Masutani (1988), while their position is shifted to the bottom of the plot, due to lower initial Péclet numbers. The slope of the IAA data fit is slightly higher than the slope of SDS data fits, due to higher migration velocity towards the interface for IAA. Tergitol data by Masutani are also included in fig. 4.9. This higher molecular weight surfactant shows a slower decline in mass transfer, a consequence of its lower migration velocity. The scatter of Tergitol points can be sub-grouped in six aligned clusters, one for each c_B , each with its $(Ro)_{I,II}$.

Surfactant migration velocity is dependent upon the chemical nature of the surfactant. In general, when approximating surfactant molecules to spheres, higher molecular weight surfactants have lower migration velocities. However, care is necessary when considering macromolecules and polycharged compounds that are likely to adopt steric configurations not assimilable to a spherical shape. Also, dissociated species such as salts or alcohols behave as gas transfer enhancers, and their solutions may show apparent gas transfer coefficients several fold the gas transfer coefficient of pure water (Zlokarnik, 1980). Yet, this effect is compensated by a much larger decline of the O_2 saturation concentration in these solutions, with a net result of decreased overall gas transfer.

Fig.4.10 shows the evolution of interfacial mass transfer during a time-dependent case in dimensionless form. Data points in this plot are selected measurements, and trendlines are power best-fits to data estimated with eq.4.6. The Sherwood number (representing mass transfer) declines over time very rapidly, a consequence of a slight decline in (Pe) (representing advection) and a rapid growth in surface contamination $(Ro)_{II}$.

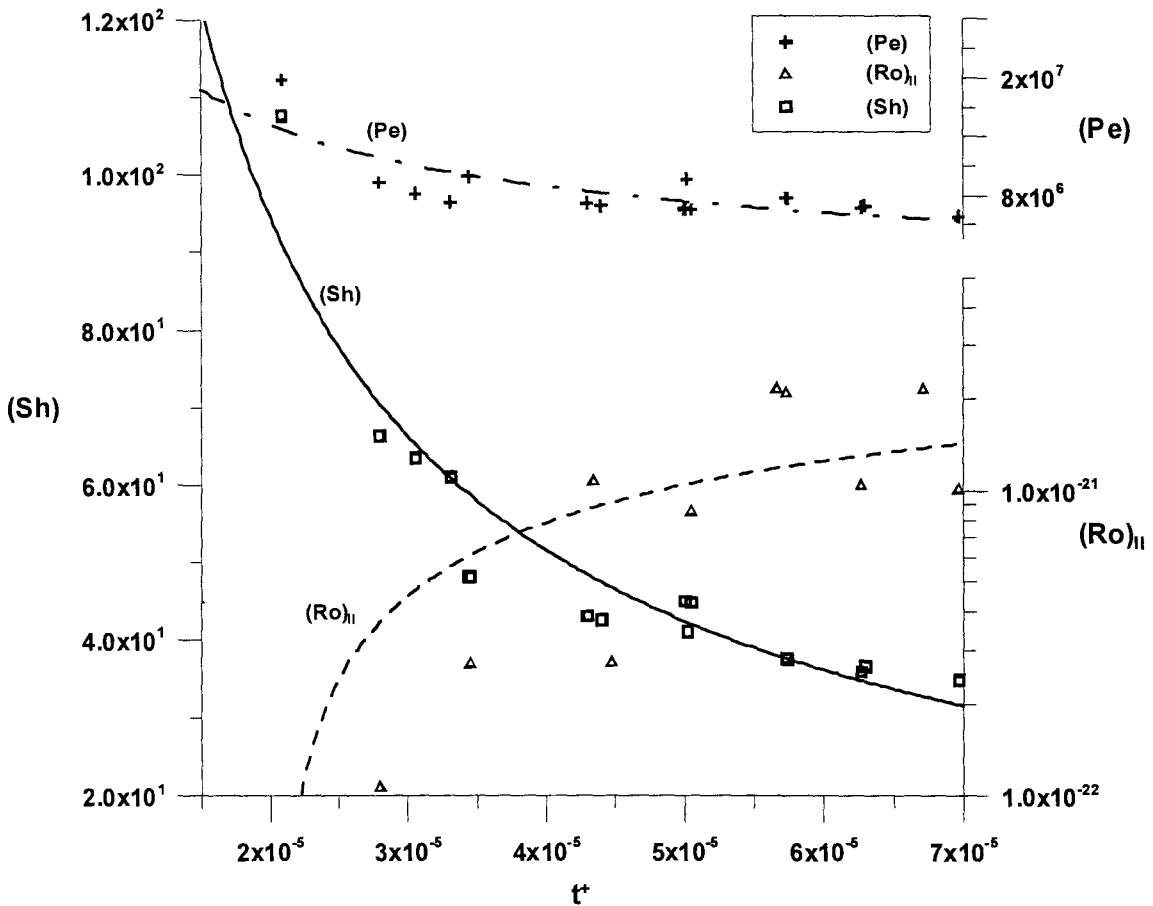


Figure 4.10. Dimensionless characterization of mass-transfer phenomena at a fine-bubble interface. (Sh) , (Pe) , and $(Ro)_{II}$ are the interfacial Sherwood, Péclet, and time-dependent contamination numbers, respectively. The slight decline in (Pe) is due to the increase in surface rigidity (hence of the drag coefficient) associated with contamination, and to the mass loss (hence lower bubble diameter) due to gas transfer. The rapid surfactant interfacial contamination process is described by $(Ro)_{II}$.

As the interface starts forming, surfactants rapidly migrate towards it, driven by van der Waals exclusion forces. This results in interfacial gas diffusivity smaller than bulk diffusivity. Although the interfacial gas diffusivity appears at the denominator in (Sh), its effect on the equation does not bias the result, as it is present in the denominator of (Pe) as well. The value of γ is known to decline with increasing time, which is accounted in the denominator of $(Ro)_{II}$.

Fig.4.11 shows a comparison of (Sh) values from experimental data, calculated with eq.4.6, and with a Frössling-like equation by Clift et al (1978). For $(Sh) > 10^2$, which correspond to the higher range of (Pe) and shorter time-limits, higher interfacial shear offset contamination effects. As (Pe) reduces in value with increasing dimensionless times, and with increasing contamination with increasing t^+ , (Sh) reduces in value and as contamination progresses, eq.4.6 better describes the data points. This shows once again that at initial times, when contamination has not yet reached a significant value, the bubble transfers oxygen to an extent comparable to a bubble in clean water.

Finally, fig.4.12 shows the limit of applicability of eq.4.6 in terms of flow regime. Eq.4.6 has an exponent for (Pe) of 1/3, which describes solid sphere approximation. This holds while contamination effects are dominant [$(Pe) < 10^7$], and for higher interfacial velocities contamination is offset by higher renewal rates. This is characterized by bubbles behaving as fluid spheres. Hence, the exponent for (Pe) in this region equals 1/2.

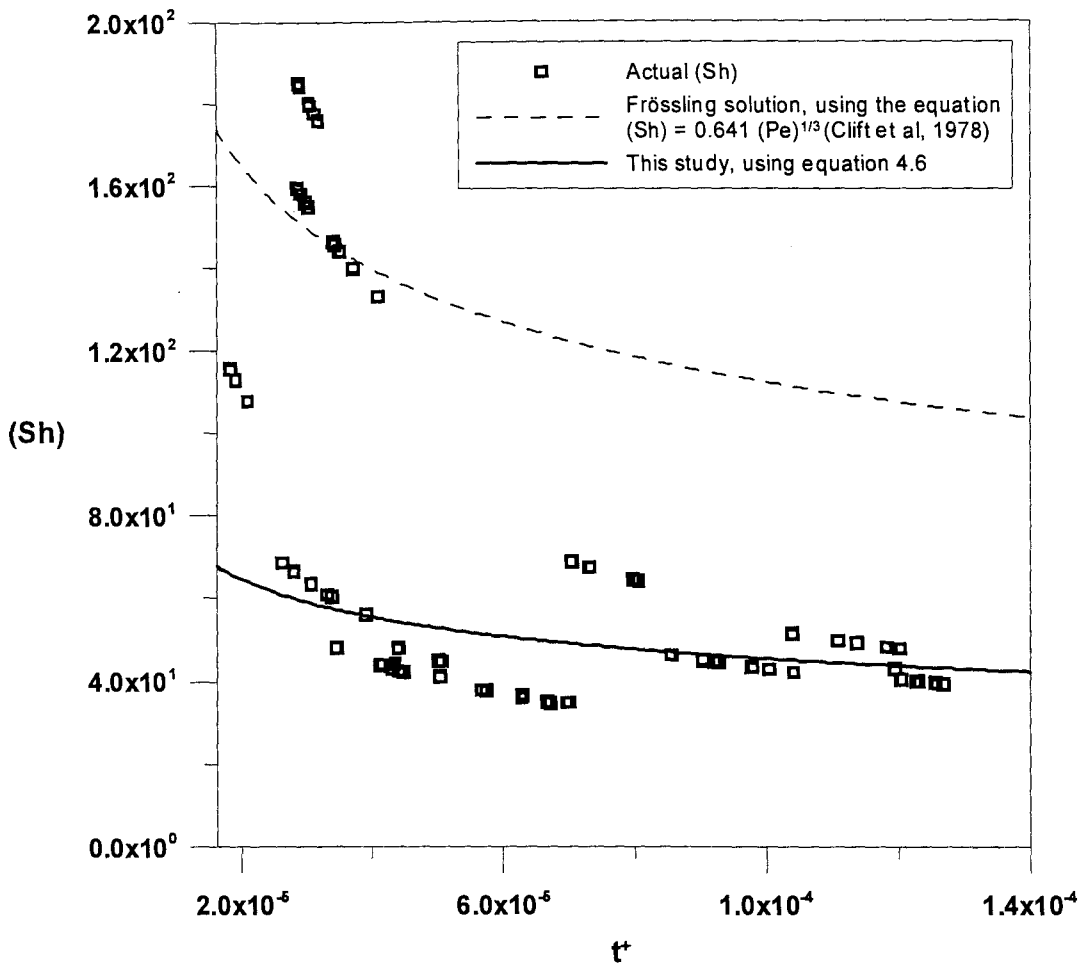


Figure 4.11. Comparison of (Sh) from experimental data, a data fit calculated with a Frössling-like equation (shown on chart, after Clift et al, 1978), and a data fit calculated with eq.4.6. Note that, as time and contamination progress, eq.4.6 better describes the reduced mass transfer.

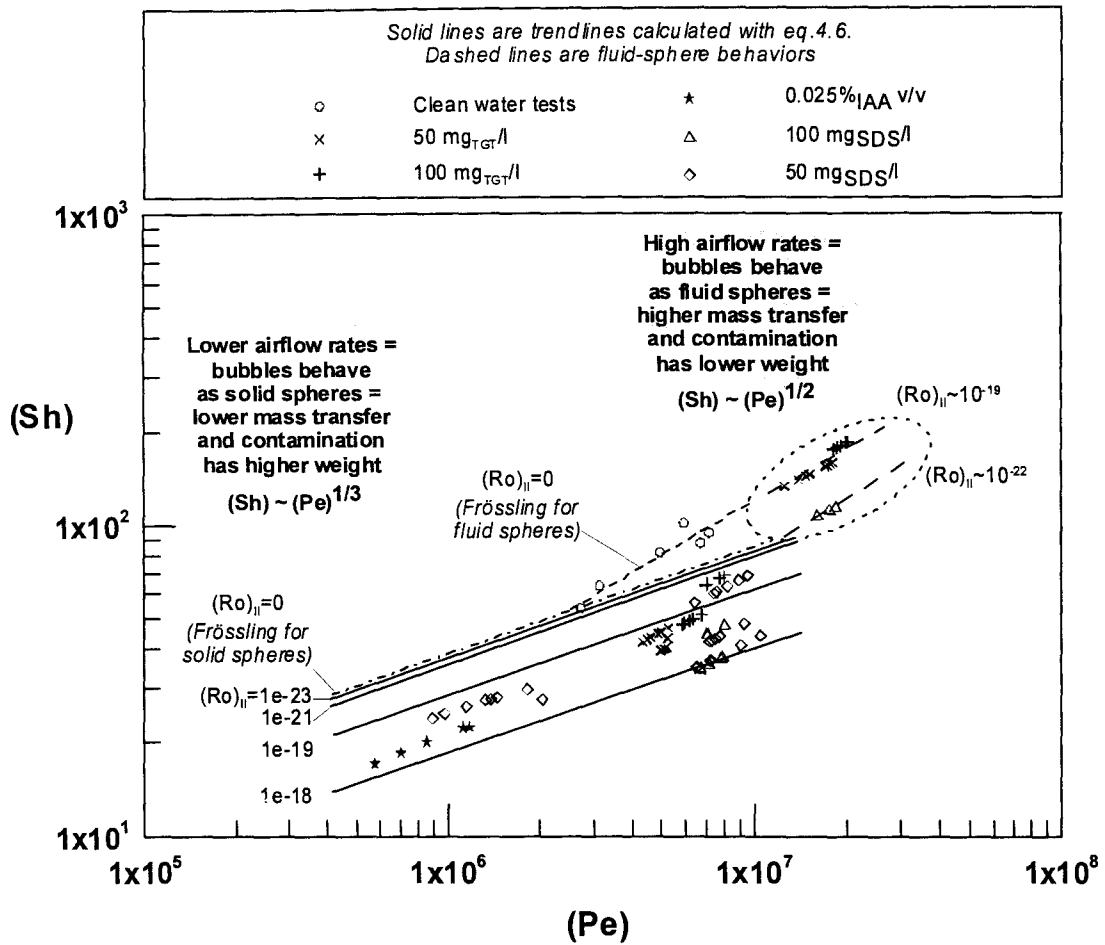


Figure 4.12. Limits of applicability of eq.4.6: (Sh) vs. (Pe)

Clean water tests show that contamination as high as $(Ro)_{II} \sim 10^{-19}$ can be offset by high flow regime: in fig.4.12 the trendline for clean water points (fluid sphere approximation) is very close to the trendline for contaminated solutions, showing the expected behavior for coarser bubbles, i.e. reduced gas transfer depression. This region corresponds to economically disadvantageous, if not unfeasible, operations in wastewater aeration.

6. SUMMARY AND CONCLUSIONS

Surface active agents are widely present in environmental applications, as well as in most industrial reactors. By accumulating at the gas-liquid interface, surface contamination results in lower surface tension, reduced interfacial renewal, and reduced gas transfer into the liquid. For a given contamination, interfaces with higher renewal rates have higher mass transfer. For a given flow regime, hence a given renewal rate, higher contaminations result in lower mass transfer. At higher renewal rates, the variation due to different contaminations is smaller than the variation at lower renewal rates. Therefore, higher flow regimes can offset contamination.

Previously in our laboratory, commercially available surfactants were used to concurrently measure dynamic surface tension and mass transfer coefficients (Masutani, 1988; Huo, 1998). In the present work all experimental data available were assembled in datasets that were analyzed, conditioned, and compiled in dimensionless form. Dynamic surface tension datasets were used to calculate interfacial contaminant accumulations with a time-dependent interfacial adsorption model.

This work has shown that the turbulence regime controls the depression of gas transfer caused by surface active agents, which is often quantified by an empirical ratio, called the α factor. The turbulence regime can be characterized by the interfacial Péclet numbers and the mass transfer by the interfacial Sherwood number. The Sherwood number can be correlated to the Péclet number to account for turbulence and to a dimensionless number,

called the interfacial contamination number, to account for interfacial contaminant accumulation.

The results explain why fine bubbles have greater mass transfer depression than coarse bubbles or droplets. The turbulence associated with coarse bubbles makes them behave more like droplets than fine bubbles. High turbulence regime interfaces may achieve better gas transfer rates, but at the expense of lower transfer efficiency (gas transferred per unit fed).

Dynamic surface tension has a direct correlation to mass transfer coefficients for all cases presented, and it is used to derive a correction to the empirical equations for gas transfer in pure liquids based on the equation by Frössling (1938). A dimensional analysis on the datasets results in correlations that quantify the evolution of mass transfer decline and interfacial contamination increase (i.e., surface tension decline) over time, which is not accounted for in Frössling-like equations. The final correlation agrees with observed transfer rates within the range of operating conditions of fine-bubbles.

7. FURTHER RESEARCH

Goal of this research was to investigate transport phenomena at contaminated gas-liquid interfaces, and provide a tool to estimate gas transfer depression caused by surface active agents. This was accomplished by means of a dimensional analysis of existing datasets.

There are available models in literature that are based on the analytical solutions of penetration theory and surface renewal models by Higbie (1935) and Danckwerts (1951), respectively. Following are suggestions for future research areas.

1. Further research on this work shall include an analytical approach to complete the logical path to derive mass transfer coefficients from dynamic surface tension measurements. The required steps to date were all analytical except for the calculation of $k_L a$ from interfacial diffusivities. A surface renewal model will refine the solutions obtained with the empirical correlations in this work.

2. An additional suggestion is to create an experimental setup that utilizes process water, containing a range of surfactants. Process water contains suspended solids, and novel applications such as membrane bio-reactors utilize process waters with suspended solid concentrations in the non-Newtonian range (Wagner et al, 2002). Tests on process water will further define the limit of applicability of the empirical correlations obtained in this study, and provide data for an additional dimensional analysis that will include viscous transport mechanisms.

8. REFERENCES

1. Aberley, R.C., Rattray, G.B. and Douglas, P.P. (1974) Air Diffusion Unit, *Journal WPCF*, v.46, no.5, pp. 895-910
2. Acrivos, A., Goddard, J.D. (1965) Asymptotic expansions for laminar forced-convection heat and mass transfer – Part 1. Low speed flows, *Journal of Fluid Mechanics*, 23, 273-291.
3. Ahmed, T., and Semmens, M.J. (1992) Use of sealed end hollow fibers for bubbleless membrane aeration: experimental studies, *J. Membr. Sci.* 69, 1-10.
4. Alves, S.S., Orvalho, S.P., Vasconcelos, J.M.T. (2005) Effect of bubble contamination on rise velocity and mass transfer. *Chemical Engineering Science*, 60, 1-9.
5. American Society of Civil Engineers - ASCE (1984, 1991). *Measurement of Oxygen Transfer in Clean Water*. ASCE 2-91, American Society of Civil Engineers, New York.
6. ASCE - American Society of Civil Engineers (1984, 1991) *Measurement of Oxygen Transfer in Clean Water*. American Society of Civil Engineers - ASCE 2-91, 345 E. 47th St, New York, New York.
7. ASCE (1997) *Standard Guidelines for In-Process Oxygen Transfer Testing*, ASCE 18-96, 345 E. 47th St, New York, NY
8. ATV-DVWK Abwassertechnische Vereinigung - Deutsche Vereinigung für Wasserwirtschaft, Abwasser und Abfall e.V. (1996) *Measurement in Clean Water and Activated Sludge of the Oxygen Transfer by Aeration Installations in Activated Sludge Plants*, Advisory Leaflet ATV-M 209 E, Deutsche Vereinigung für Wasserwirtschaft, Abwasser und Abfall e.V., Wuppertal.
9. Azbel, D. (1981) *Two-phase flows in chemical engineering*, Cambridge University Press, Cambridge.
10. Bailey, J.E., Ollis, D.F. and Bayley, J. (1986) *Biochemical Engineering Fundamentals – 2nd ed.*, McGraw-Hill, New York
11. Bass, S.J., and Shell, G.L. (1977) Evaluation of oxygen transfer coefficients of complex wastewaters, *Proc. 32nd Industrial Waste Conf., Purdue University, Lafayette, IN*.
12. Batchelor, G.K. (1967) *An Introduction to Fluid Dynamics*, Cambridge University Press, Cambridge (UK)
13. Bhaga, D. and Weber, M.E. (1981) Bubbles in Viscous Fluids: Shapes, Wakes and Velocities, *J. Fluid Mech.*, 105: 61-85

14. Bird, R.B., Steward, W.E. and Lightfoot, E.N. (1960) Transport Phenomena, *John Wiley & Sons*, New York
15. Bohr, N. (1909) Determination of the Surface Tension of Water by the Method of Jet Vibration, *Roy. Soc. London, Phil. Trans. Ser. A*, 209: 281-317
16. Boussinesq, J. (1913) Vitesse de la chute lente, devenue uniforme, d'une goutte liquide sphérique, dans un fluide visqueux de poids spécifique moindre. *Annales de Chimie et de Physique*, 29, 364-372.
17. Burcik, E.J. (1950) The Rate of Surface Tension Lowering and its Role in Foaming, *J. Colloid Sci.*, 5: 421-436
18. Calderbank, P.H., Johnson, D.S.L. and Loudon, J. (1970) Mechanics and Mass Transfer of Single Bubbles in Free Rise Through Some Newtonian and Non-Newtonian Liquids, *Chem. Eng. Sci.*, 25: 235-256
19. Capela, S., Roustain, M. and Héduit, A. (2001) Transfer Number in Fine Bubble Diffused Aeration Systems, *Wat. Sci. Tech.*, 43 (11): 145-152
20. Carver, C.E., Jr. (1969) Oxygen Transfer from Falling Water Droplets, *J. San. Eng. Div. – Proc. ASCE*, 95 (No Sa2): 239-251
21. Caskey, J.A. and Barlage, W.B., Jr. (1971) An Improved Experimental Technique for Determining Dynamic Surface Tension of Water and Surfactant Solutions, *J. Colloid and Interface Sci.*, 35: 46-52
22. Chang, C.-H. and Franses, E.I. (1994) Dynamic Tension Behavior of Aqueous Octanol Solutions under Constant-Area and Pulsating-Area Conditions, *Chem. Eng. Sci.*, 49 (3): 313-325
23. Chern, J.-M. and Yu, C.F. (1997) Oxygen Transfer Modeling of Diffused Aeration Systems, *Ind. Eng. Chem. Res.*, 36: 5447-5453
24. Chern, J.-M., Chou, S.-H. and Shang, C.-S. (2001) Effects of Impurities on Oxygen Transfer Rates in Diffused Aeration Systems, *Wat. Res.*, 35 (13): 3041-3048
25. Chindanonda, S. (2002) Estimating Oxygen Transfer Coefficients in the Presence of Surfactants, thesis presented to Chulalongkorn University, Thailand, in partial fulfillment of the requirements for the degree of Master of Science
26. Clift, R., Grace, J. R., and Weber, M. E. (1978) *Bubbles, Drops and Particles*; Academic Press: New York.
27. Côté, P., Bersillon, J.-L., and Huyard, A. (1989) Bubble-free aeration using membranes: mass transfer analysis, *J. Membr. Sci.* 47, 91-106.
28. Crooks, R., Cooper-White, J. and Boger, D.V. (2001) The Role of Dynamic Surface Tension and Elasticity on the Dynamics of Drop Impact, *Chem Eng. Sci.*, 56: 5575-5592

29. Danckwerts, P.V. (1951) Significance of Liquid-Film Coefficients in Gas Absorption, *Ind. Eng. Chem.*, 43 (6): 1460-1467
30. Danckwerts, P.V. (1970) Gas-Liquid Reactions, *McGraw-Hill*, New York
31. Daniel, R.C., Berg, J.C. (2001) Diffusion-Controlled Adsorption at the Liquid-Air Interface: The Long-Time Limit, *Journal of Colloid and Interface Science*, 237, 294-296.
32. Daniel, R.C., Berg, J.C. (2003) A simplified method for predicting the dynamic surface tension of concentrated surfactant solutions, *Journal of Colloid and Interface Science*, 260, 244-249.
33. Datwani, S.S., Stebe, K.J. (2001) Surface Tension of an Anionic Surfactant: Equilibrium, Dynamics, and Analysis for Aerosol-OT, *Langmuir*, 17, 4287-4296.
34. Davis, J.T. (1977) Diffusion and Heat Transfer at Boundaries of turbulent Liquids, *Physiochemical Hydrodynamics (by Levich, V.G.; D.B. Spalding ed.) Advance Publications Ltd.*, London, UK, 3-22
35. Davis, J.T. and Rideal, E.K. (1961) Interfacial Phenomena – 2nd ed., Academic Press, London, UK
36. De Kee, D. and Chhabra, R.P. (2002) Transport Processes in Bubbles, Drops, and Particles - 2nd ed., *Taylor & Francis*, New York
37. Eckenfelder, W. W., and Ford, D. L. (1968) New concepts in oxygen transfer and aeration, *Advances in water quality improvement, E. F. Gloyna, and W. W. Eckenfelder Jr. (eds.)*, University of Texas Press, Austin, Tex., 215-236
38. Eckenfelder, W.W. (1959) Absorption of oxygen fro air bubbles in water, *Journal of the Sanitary Engineering Division Proceedings of the American Society of Civil Engineers*, 2090, 89-99.
39. Eckenfelder, W.W., and Barnhart, E. L. (1961) The Effect of Organic Substances on the Transfer of Oxygen from Air Bubbles in Water, *AIChE J.*, 7(4), 631-634.
40. Eckenfelder, W.W., Jr., Raymond, L.W. and Lauria, D.T. (1956) Effect of various organic substances on oxygen adsorption efficiency, *Sewage and Industrial Wastes J.*, 28 (11): 1357-1364
41. Edwards, D.A., Brenner, H. And Wasan, D.T. (1991) Interfacial Transport Processes and Rheology, *Butterworth-Heinemann Series in Chemical Engineering*, Stonham, MA
42. Fainerman, V.B., Miller, R. and Joos, P. (1994) The Measurement of Dynamic Surface Tensions of Highly Viscous Liquids by the Maximum Bubble Pressure Method, *Colloids and Surfaces A: Pshysiochemical and Engineering Aspects*, 75: 229-235

43. Fan, L.-S. and Tsuchiya, K. (1990) Bubble Wake Dynamics in Liquids and Liquid-Solid Suspensions, *Butterwoth-Heinemann*, Stonheam, MA
44. Ferri, J.K., Stebe, K.J. (2000) Which surfactants reduce surface tension faster? A scaling argument for diffusion-controlled adsorption, *Advances in Colloids and Interface Science*, 85, 61-97.
45. Freud, B.B. and Freud, H.Z. (1930) A theory of the ring method for the determination of surface tension, *Journal of the American Chemical Society*, 52, 1772-1782.
46. Friedlander, S.K. (1957) Mass Transfer to Single Spheres and Cylinders at Low Reynolds Numbers, *AIChE J.*, 3: 43-48
47. Friedlander, S.K. (1961) A Note on Transport to Spheres in Stokes Flow, *AIChE J.*, 7: 347-348
48. Frössling, N. (1938) Über die Verdunstung fallender Tropfen, *Gerlands Beiträge zur Geophysik*, 52: 170–215
49. Fujimoto, T. (1985) New Introduction to Surface Active Agents, *Sanyo Chemical Industries Ltd.*, Kyoto (Japan)
50. Garner, F.H., and Hammerton, D. (1954) Circulation inside gas bubbles, *Chem. Eng. Sci.*, 8(1), 1-11.
51. Gibbs, J. W. (1928) Collected Works, *Longmans, Green and Co.*, New York
52. Griffith, R.M. (1960) The effect of surfactants on the terminal velocity of drops and bubbles. *Chemical Engineering Science*, 12, 198-213.
53. Haberman, W.L. and Morton, R.K. (1953) An Experimental Investigation of the Drag and Shape of Air Bubbles Rising in Various Liquids, *D.W. Taylor Model Basin Report 802*, Navy Dept., Washington, DC
54. Haberman, W.L. and Morton, R.K. (1954) An Experimental Study of Bubbles Moving in Liquids, *Proc. ASCE*, 387: 227-252
55. Hansen, R.S. (1960) The theory of diffusion controlled absorption kinetics with accompanying evaporation, *Journal of Physical Chemistry*, 64, 637-641.
56. Harkins, W. D. and Jordan, H. F. (1930) A method for the determination of surface and interfacial tension from the maximum pull on a ring, *J. ACS*, 52: 1751-1772
57. Harkins, W.D. (1952) The Physical Chemistry of Surface Films, *Reinhold Press*, New York
58. Higbie, R. (1935) The rate of absorption of a pure gas into a still liquid during short periods of exposure, *AIChE Trans.*, 31: 365-388
59. Huo, T.L. (1998) The Effect of Dynamic Surface Tension on Oxygen Transfer Coefficient in Fine Bubble Aeration System, thesis presented to University of

California, at Los Angeles, CA, in partial fulfillment of the requirements for the degree of Doctor of Philosophy

60. Hwang, H.J., and M.K. Stenstrom (1979) *The Effect of Surface Active Agents on Oxygen Transfer*, UCLA-ENG-79-30, University of California, Los Angeles.
61. Johnson, A.I., Hamielec, A.E. and Houghton, W.T. (1967) An Experimental Study of Mass Transfer with Chemical Reaction from Single Gas Bubbles, *Can. J. Chem. Eng.*, 45: 140
62. Kessener, H. J. and Ribbius, F. J. (1935) Practical Activated Sludge Research. *J. Proc. Inst. Sew. Purification*, 6(3), 50–56.
63. Kloubek, J. (1972a) Measurement of the Dynamic Surface Tension by Maximum bubble Pressure Method. III. Factors Influencing the Measurement at High Frequency of Bubble Formation and an Extension to Zero Age of Surface, *J. Colloid Interface Sci.*, 41: 7-16
64. Kloubek, J. (1972b) Measurement of the Dynamic Surface Tension by Maximum bubble Pressure Method. IV. Surface Tension of Aqueous Solutions of Sodium Dodecyl Sulfate, *J. Colloid Interface Sci.*, 41: 17-32
65. Kunii, D. and Levenspiel, O. (1969) *Fluidization Engineering*, John Wiley & Sons, New York
66. Lamont, J.C., and Scott, D.S. (1970) An Eddy Cell Model of Mass Transfer into the Surface of a Turbulent Liquid, *AIChE J.*, 16, 513-519.
67. Lecomte du Noüy, P. (1919) A New Apparatus for Measuring Surface Tension, *J. Gen. Physiol.*, 1: 521-524
68. Lee, Y.-L. (2003) Surfactant Effects on Mass Transfer During Drop-Formation and Drop Falling Stages, *AIChE J.*, 49 (7): 1859-1869
69. Levich, V.G. (1959) *Fiziko-khimicheskai a gidrodinamika – Izd. 2, Gos izd-vo fiziko-matematicheskoi lit-ry*, Moskva (SSSR)
70. Levich, V.G. (1962) *Physicochemical hydrodynamics* (2nd ed.). Prentice-Hall, New York.
71. Lewis, W. K., and Whitman, W. G. (1924) Principles of gas adsorption, *Ind. Engr. Chem.*, 16 (12): 1215-1220
72. Libra, J.A. (1993) Stripping of Organic Compounds in an Aerated Stirred Tank Reactor, *VDI – Verlag GmbH*, Dusseldorf (D).
73. Liger-Belair (2003) More on the Surface State of Expanding Champagne Bubbles, *Langmuir* 19, 801-808.

74. Liu, J., Wang, C., Messow, U. (2004) Adsorption kinetics at air/solution interface studied by maximum bubble pressure method, *Colloid and Polymer Science*, 283, 139-144.
75. Llorens, J., Mans, C. and Costa, J. (1988) Discrimination of the Effects of Surfactants in Gas Absorption, *Chem. Eng. Sci.*, 43 (3): 443-450
76. Mancy, K. H., and Barlage, W. E., Jr. (1968) Mechanism of Interference of Surface Active Agents With Gas Transfer in Aeration Systems, *Advances in water quality*, F. Gloyna and W. W. Eckenfelder Jr. (eds.), University of Texas Press, Austin, TX, 262-286
77. Mancy, K.H., and Okun, D.A. (1960) Effects of Surface Active Agents on Bubble Aeration, *J. Water Poll. Cont. Fed.*, 32(4), 351-364.
78. Marangoni, C. (1871) Über die Ausbreitung der Tropfen einer Flüssigkeit auf der Oberfläche einer anderen. *Annalen der Physik und Chemie*, CXLIII(7), 337-354.
79. Marangoni, C. (1872) Sul principio della viscosità superficiale dei liquidi stabilito dal Sig. J. Plateau, *Nuovo Cimento*, II(V-VI), 239-273.
80. Marucci, G. and Nicodemo, L. (1967) Coalescence of Gas Bubbles in Aqueous Solutions of Inorganic Electrolytes, *Chem. Eng. Sci.*, 22: 1257-1265
81. Masutani, G. K. (1988) Dynamic Surface Tension Effects on Oxygen Transfer in Activated Sludge, thesis presented to University of California, at Los Angeles, CA, in partial fulfillment of the requirements for the degree of Doctor of Philosophy
82. Masutani, G., and Stenstrom, M. K. (1990). *Fine Pore Diffuser Fouling: The Los Angeles Studies*. UCLA ENG 90-02, University of California, Los Angeles.
83. Masutani, G., and Stenstrom, M.K. (1991) Dynamic Surface Tension Effects on Oxygen Transfer, *J. Environ. Eng.*, 117(1), 126-142.
84. McGinnis, D.F. and Little, J.C. (2002) Predicting Diffused-Bubble Oxygen Transfer Rate Using the Discrete-Bubble Model, *Wat. Res.*, 36: 4627-4635
85. McKeown, J.J., and Okun, D.A. (1961) Effects of surface-active agents on oxygen bubble characteristics, *Int. J. Air. Wat. Poll.* 5(2-4), 113-122.
86. Metcalf & Eddy, Inc. (2003). *Wastewater Engineering: Treatment and Reuse - 4th edn.* (Tchobanoglous, G., Burton, F.L. and Stensel, H.D. eds.). McGraw-Hill series in civil and environmental engineering, New York.
87. Miles, G.D., Shedlovsky, L. (1944) Minima in surface tension-concentration curves of solutions of sodium alcohol sulfates, *Journal of Physical Chemistry*, 48, 57-62.
88. Moore, D.W. (1959) The Rise of a Gas Bubble in a Viscous Fluid, *J. Fluid Mech.*, 6: 113-130

89. Motarjemi, M. and Jameson, G.J. (1978) Mass Transfer from Very Small Bubbles – The Optimum Bubble Size for Aeration, *Chem. Eng. Sci.*, 33: 1415-1423
90. Noskov, B.A. (1996) Fast Adsorption at the Liquid-Gas Interface, *Adv. Colloid Interface Sci.*, 69: 63-129
91. Perry, R.H., (1997) Perry's Chemical Engineers Handbook 7th ed. (D.W.Green ed.), *McGraw-Hill*, New York
92. Philichi, T. and Stenstrom, M.K.(1989) The Effect of Dissolved Oxygen Probe Lag Upon Oxygen Transfer Parameter Estimation, *Journal of the Water Pollution Control Federation* 61 83-86.
93. Pierson, F.W. and Whitaker, S. (1976) Studies of the Drop-weight Method for Surfactant Solutions. II. Experimental Results for Water and Surfactant Solutions, *J. Colloid Interface Sci.*, 54: 219-230
94. Prandtl, L. (1934) Fundamentals of Hydro- and Aeromechanics (O.G. Tietjens ed.), *McGraw-Hill*, New York
95. prEN 12255-15 - European Standard (1999) Wastewater treatment plants – part 15: Measurement of the oxygen transfer in clean water in activated sludge aeration tanks (Prédiction des capacités d'oxygénation en eau claire des systèmes d'insufflation d'air), NormAPME, Brussels.
96. Ramirez, J.A., and Davis, R.H. (1999) Mass Transfer to a Surfactant-Covered Bubble or Drop, *AIChE J.* 45(6), 1355-1358.
97. Rayleigh, Lord J. W. S. (1878) On the Instability of Jets, *Proc. London Math. Soc.*, 10: 4-13
98. Rayleigh, Lord J. W. S. (1879) On the Capillary Phenomena of Jets, *Proc. Roy. Soc.*, 29: 71-97
99. Reardon, D.J. (1995) Turning down the power, *Civ. Eng.* 65(8) 54-56.
100. Redmon, D.T., Boyle, W.C. and Ewing, L. (1983). Oxygen Transfer Efficiency Measurements in Mixed Liquor Using Off-Gas Techniques. *J. Wat. Pollut. Control Fed.* 55, 1338–1347.
101. Rillaerts, E., Joos, P. (1982) Rate of Demicellization from the Dynamic Surface Tension of Micellar Solutions, *Journal of Physical Chemistry*, 86, 3471-3478.
102. Rittman, B and McCarty, P.L. (2000) Environmental Biotechnology: Principles and Applications – 2nd ed., *McGraw-Hill*, New York
103. Rodrigue, D., De Kee, D. and Fong, C.M.C.F. (1996) An Experimental Study on the Free Rise Velocity of Gas Bubbles, *J. Non-Newtonian Fluid Mech.*, 66: 213-232
104. Rosen, M.J. (1978) Surfactants and Interfacial Phenomena. John Wiley & Sons, New York.

105. Rosso, D., and Stenstrom, M.K. (2005a) Comparative Economic Analysis of the Impacts of Mean Cell Retention Time and Denitrification on Aeration Systems, *Wat. Res.*, **39**, 3773-3780.
106. Rosso, D., and Stenstrom, M.K. (2005b) Economic Implications of Fine Pore Diffuser Aging, *Wat. Environ. Res.*, in press.
107. Rosso, D., and Stenstrom, M.K. (2005c) Surfactant Effects on Alpha Factors in Aeration Systems, *Wat. Res.*, submitted.
108. Rosso, D., Iranpour, R. and M.K. Stenstrom, (2001) Fine Pore Aeration - Fifteen Years of Off-Gas Transfer Efficiency Measurements, *Proc. WEFTech WEF Conf.*, Atlanta, GA, October 2001
109. Rosso, D., Iranpour, R. and Stenstrom, M.K. (2005). Fifteen Years of Off-gas Transfer Efficiency Measurements on Fine-Pore Aerators: Key Role of Sludge Age and Normalized Air Flux. *Wat. Environ. Res.* **77**(3), 266-273.
110. Roy, S., and Duke, S.R. (2004) Visualization of oxygen concentration fields and measurement of concentration gradients at bubble surfaces in surfactant-contaminated water, *Experiments in Fluids*, **36**, 654-662.
111. Sadhal, S.S., Johnson, R.E. (1983) Stokes-flow past bubbles and drops partially coated with thin-films .1. Stagnant cap of surfactant film - exact solution. *Journal of Fluid Mechanics*, **126**, 237-250.
112. Savart, F. (1833) Memoire sur la Constitution des Veines Liquides Lancees par des Orifices Circulaires en Mince Paroi, *Annales de Chimie et de Physique*, **53**: 337-386
113. Semmens, M.J. (1990) *Bubbleless gas transfer device and process*, United States Patent No. 5,034,164.
114. Sherwood, T.K., Pigford, R.L. and Wilke, C.R. (1975) *Mass Transfer*, McGraw-Hill, New York
115. Springer, T.G. and Pigford, R.L. (1970) Influence of Surface Turbulence and Surfactants on Gas Transport Through Liquid Interfaces, *Ind. Eng. Chem. Fundam.*, **9** (3): 458-465
116. Stenstrom, M. K., and Gilbert, R. G. (1981) Effects of Alpha, Beta, and Theta Factors upon the Design, Specification, and Operation of Aeration Systems, *Wat. Res.*, **15** (6): 643-654
117. Stenstrom, M.K., Brown, L.C. and Hwang, H.J. (1981) Oxygen Transfer Parameter Estimation, *J. Env. Eng. Div. ASCE*, **121**: 858-866
118. Stukenberg, J.R., Wahbeh, V.N., and McKinney, R.E. (1977) Experiences in evaluating and specifying aeration equipment, *J. Wat. Poll. Contr. Fed.* **49**(1), 66-82.

119. Sudgen, S. (1922) Determination of Surface Tension from the Maximum Pressure in Bubbles, *J. Chem. Soc.*, 121: 858-866
120. Sudgen, S. (1924) Determination of Surface Tension from the Maximum Pressure in Bubbles - Part II, *J. Chem. Soc.*, 125: 27-31
121. Tadros, Th.F. (ed.) (1984) Surfactants, *Academic Press*, London, UK
122. Treybal, R.E. (1968) Mass-Transfer Operations - 2nd ed., *McGraw-Hill*, New York
123. Tzounakos, A.m Karamanev, D.G., Margaritis, A., and Bergougnou, M.A. (2004) Effect of the Surfactant Concentration on the Rise of Gas Bubbles in Power-Law Non-Newtonian Liquids, *Ind. Eng. Chem. Res.* **43**, 5790-5795.
124. US EPA (1985) Fine Pore (Fine Bubble) Aeration Systems, EPA/625/8-85/010, Cincinnati, OH
125. US EPA (1989) Fine Pore (Fine Bubble) Aeration Systems, EPA/625/1-89/023, Cincinnati, OH
126. Vasconcelos, J.M.T., Orvalho, S.P. and Alves, S.S. (2002) Gas-Liquid Mass Transfer to Single Bubbles: Effect of Surface Contamination, *AIChE J.*, 48 (6): 1145-1154
127. Wagner, M. and Pöpel, H.J. (1996) Surface Active Agents and Their Influence on Oxygen Transfer, *Wat. Sci. Tech.*, 34 (3-4): 249-256
128. Wagner, M., Cornel, P, and Krause, S. (2002) Efficiency of different aeration systems in full scale membrane bioreactors, *Proc. 75th WEFTEC conference, Chicago, IL.*
129. Ward, A.F.H., Tordai, L. (1946) Time-Dependence of Boundary Tensions of Solutions I. The Role of Diffusion in Time-Effects, *The Journal of Chemical Physics*, 14, 453-461.
130. Wasekar, V.M. and Manglik, R.M. (2003) Short-Time-Transient Surfactant Dynamics and Marangoni Convection Around Boiling Nuclei, *Trans. ASME*, 125, 858-866.
131. Weber, M.E. (1975) The effect of surface active agents on mass transfer from spherical cap bubbles. *Chemical Engineering Science*, 30, 1507-1510.
132. Zlokarnik, M. (1969) Application of the Theory of Similarity to the solution of mixing problems, *Proc. CHISA Congress, Marianske (CZ)*
133. Zlokarnik, M. (1977) Influence of Some Important Geometric, Material and Process Parameters on Mass Transfer in Gas-Liquid Contacting, *Proc. of the Conference "Mass Transfer and Scale-Up of Fermentations"*, Hennicker, N.H. (D), July 1977

134. Zlokarnik, M. (1978a) Influence of Various Material and Process Related Parameters on Bubble Coalescence in Gas/Liquid Contacting, *Proc. 1st European Congress on Biotechnology*, CH-Interlaken, September 1978
135. Zlokarnik, M. (1978b) Sorption Characteristics for Gas-Liquid Contacting in Mixed Vessels, *Adv. Biochem. Eng.*, 8: 133-151
136. Zlokarnik, M. (1979) Sorption Characteristics of Slot Injectors and Their Dependency on the Coalescence Behaviour of the System, *Chem. Eng. Sci.*, 34: 1265-1271
137. Zlokarnik, M. (1980a) Koaleszenzphänomene im System gasförmig/flüssig und deren Einfluß auf den O₂-Eintrag bei der biologischen Abwasserreinigung, *Korresp. Abw.*, 27(11), 728-734.
138. Zlokarnik, M. (1980b) Eignung und Leistungsfähigkeit von Oberflächenbelüftern für biologische Abwasserreinigungsanlagen, *Korresp. Abw.*, 27(1), 14-21.
139. Zlokarnik, M. (1980b) Koaleszenzphänomene im System gasförmig/flüssig und deren Einfluß auf den O₂-Eintrag bei der biologischen Abwasserreinigung, *Korrespondenz Abwasser*, 27 (11): 728-734
140. Zlokarnik, M. (2002) *Scale-Up in Chemical Engineering*. Wiley-VCH, Weinheim.